AEDC-TR-73-111

FIBER OPTICS PARTICLE-SIZING SYSTEM

H. T. Bentley

ARO, Inc.

September 1973

ARNOLD ENGINEERING DEVELOPMENT CENTER
AIR FORCE SYSTEMS COMMAND
ARNOLD AIR FORCE STATION, TENNESSEE

NOTICES

FIBER OPTICS PARTICLE-SIZING SYSTEM

H. T. Bentley

ARO, Inc.

FOREWORD

The work reported herein was conducted by the Arnold Engineering Development Center (AEDC), Air Force Systems Command (AFSC), under Program Element 65802F.

The results of research presented were obtained by ARO, Inc. (a subsidiary of Sverdrup & Parcel and Associates, Inc.), contract operator of AEDC, AFSC, Arnold Air Force Station, Tennessee. The research was conducted from July 1971 to June 1972 under ARO Project No. BB5252. The manuscript was submitted for publication on April 25, 1973.

The author wishes to acknowledge the efforts of D. C. Todd in the programming and V. A. Cline in both the theoretical and the experimental studies represented in this report.

This technical report has been reviewed and is approved.

MAURICE A. CLERMONT
Major, CF
Research and Development Division
Directorate of Technology

ROBERT O. DIETZ
Director of Technology

ABSTRACT

A fiber optics particle-sizing system is discussed with respect to theory of operation and data acquisition and reduction techniques. The system utilizes a shadowgraphic technique to determine the dimensions and numbers of particles moving in a flow field. The system is digital in nature. Particles pass through a collimated laser beam and are imaged onto a linear array by a coaxial lens. The array is composed of the exposed ends of a fiber optics bundle which serves as a "link" between the array plane and the sensing photo-detector modules. Being an imaging device, it can measure a wide range of particle sizes through the proper selection of optics. Sizes ranging from 2 to 1500 μm have been measured in the course of this project. Comparisons of holographic data of a liquid rocket injector and of water spray nozzles are made with the fiber optics system.

CONTENTS

APPENDIXES

I. ILLUSTRATIONS

Figure

NOMENCLATURE

A	Area of overlap
b	Bin size
C	Depth-of-field constant
D	Particle diameter
D_{30}	Volume mean diameter
d	Diameter
$d_{\pm}$	Coordinates of particle edges
F	Defined in Nukiyama-Tanasawa analysis
f	Distribution function

f/	Focal length
Im	Imaginary part
I_0	Modified Bessel function of zeroth order
J	An integer, Bessel function
j	Imaginary unit (-1), particle flux
K	Probability variable
k	Propagation constant
L	Effective depth of field
ℓ	Lens diameter
M	Magnification
N	Number of counts in a channel
n	Number density cm^{-3}
P	Power, count probability
R	Ratio of numerical apertures
Re	Real part
r	Radial coordinate
T	Sample time
t	Sample volume thickness
u	Amplitude of light disturbance
V	Particle velocity
W	Effective array width
w	Beam width of Gaussian at $1/e^2$ point
X	Length of array
x, y, z	Coordinates
α	Intensity ratio, longitudinal
β	Intensity ratio, radial
γ	Number of array elements
Δ	Defined in Fig. 7
ΔR	Volume fraction

ϵ	Fraction of a bin size
θ	Angle
λ	Wavelength
ξ	Probability of triggering
τ	Characteristic time of particles
Ω	Input beam width of Gaussian at $1/e^2$ point

SUBSCRIPTS

D	Disk
f	Fiber
h	hole
i	Size channel designation
ℓ	X
m	Diameter, maximum

SECTION I
INTRODUCTION

1.1 PROGRAM OBJECTIVE

The objective of this program is to provide system evaluation of a particulate-monitoring system selected under Project BB513 (Particle Contamination Sensor in High-Temperature Regeneratively Heated Wind Tunnels). The program objectives called for the monitoring of the size distribution and particle flux of ceramic contaminants emitted from a large, ceramic-filled storage heater, with specific application to the Aerodynamic Propulsion Test Unit (APTU). These contaminants are produced from the heat exchanger materials by thermal shock and by the mechanical abrasion which occurs during the heating and cooling cycles. Particulate contaminants in the test flow could cause surface damage to a test model and also be a source of test data error. A continuous contamination monitor could provide contamination level information necessary for correcting the test data. Such a system could also provide heater bed information and perhaps aid in the forecast of impending structural failure of the bed by noting changes in the dusting rate or size distribution. If detected in time, some deterioration can be repaired by heat treatment.

The initial program was subdivided into the five following tasks:

1. Determine the approximate size and quantity of contaminants expected from such heaters.

2. Determine the particle size and concentration that would be detrimental to wind tunnel operations.

3. Describe the environment in which the device will operate.

4. Survey the available devices, or techniques, for this purpose and choose the one most suitable.

5. Evaluate the system operation.

Under Project BF5135 the first four tasks were completed and the fiber optics system (FOS) was finally chosen as providing immediate promise for application under the unfavorable operation conditions to be encountered. The system had to operate in an extreme temperature, velocity, and pressure environment which was made more untenable by the presence of density gradients.

1.2 ELECTRO-OPTICAL TECHNIQUE

The electro-optical technique was originally developed and reported (Ref. 1) by personnel at the National Center for Atmospheric Research, Boulder, Colorado. The device was used for measurements of size distributions of cloud and precipitation particles in the range from 5 to 1000 μm at low, subsonic aircraft speeds. The speeds expected in tunnel application were an order of magnitude higher, while the same size range was to be measured. For this reason Transistor-Transistor Logic (TTL) electronics and photomultiplier (PM) tubes were used for the detector system. At the time, this combination promised the fastest response, which was approximately 30 MHz. A detailed description of the system electronics operation is outlined in Section 5.1, Theory of Operation.

This report will be concerned with the application of the basic instrument to tests at the Arnold Engineering Development Center (AEDC). Emphasis was placed on system performance in typical wind tunnel conditions. Data reduction methods were developed, correcting for such factors as depth of field, effective array width, average particle velocity, and counting time. Finally the results of two typical applications, a water spray droplet study and a Propulsion Wind Tunnel Facility (PWT) Dust Erosion Study, including instrumentation, will be discussed.

SECTION II
PARTICLE SAMPLING

In general, particle-sampling techniques perform spatial and temporal averages of the particulates. All techniques will sample over a region in space and time. Transient events, if they are to be time resolved, require fast sampling rates. A large number of repetitions of the event or large sample volumes are required to obtain significant counting statistics. If the process is quasi continuous, sufficiently good time averages may be obtained over a relatively small sample area. APTU and other continuous tunnels fall into this category. The FOS is eminently suited for this type of application, as it provides rapid counting over an area and provides a continuous update of particle size information.

For an understanding of the problem, the following two basic cases shall be discussed: (I) a spatially averaged particle size distribution obtained in one instant of time and (II) a time average distribution taken as average over an area in space. The difference between the two distributions is considerable under certain conditions.

Case I deals with scanning by photography, holography, and other short-time procedures (Ref. 2). These techniques record a volume of the flow in a period of time which is short with respect to the characteristic time of the particles, τ, to prevent blurring (Fig. 1, Appendix I).

$$\tau = \frac{D}{V}$$

where D = particle diameter and V = particle velocity. The distribution obtained from such a procedure is density weighted (i.e., the distribution function gives just the average number density of particles of a particle size).

$$n(D) \, \frac{\text{number}}{\text{volume}}$$

Case II requires real-time particle analyzers, including the FOS. Although for analysis purposes the latter contains also a sampling volume, one can assume that the volume is replaced by an area through which the particle flux streams (Fig. 2). Each particle falls into a velocity range $V_i = \overline{V}_i \pm \Delta V_i$ and a diameter range $D_i = \overline{D}_i \pm \Delta D_i$ associated with it. As each particle is swept into the active area, it is sized by some means. The resulting distribution is weighted by the particle flux as follows:

$$j_i(D) = \frac{\text{number}}{\text{area-sec}}$$

The two distributions are not independent, as they are related by the continuity equation. If the volumes are assumed to be infinitesimally small, the continuity equation is written as

$$\text{div } n\vec{V} = \frac{-dn}{dt} = \frac{\partial V_1}{\partial x} + \frac{\partial V_2}{\partial y} + \frac{\partial V_3}{\partial z}$$

Note that n and V are functions of D. Assuming steady-state particle fields, the continuity equation reduces to

$$\text{div } n\vec{V} = 0$$

$$\text{where} \quad V_1 \hat{\imath} + V_2 \hat{\jmath} + V_3 \hat{k} = \vec{V}$$

3

or

$$n\vec{V} = \vec{J} = \text{Constant}$$

Therefore, the number density of case I systems is related to the particle flux of case II systems by the particle velocity. In most applications where the flow is obtained by the acceleration of a gas through a nozzle or around a model, one can not expect to have an equilibrium between particle and gas velocity fields. Since drag is a surface effect and inertial forces are volume dependent, a velocity distribution would be expected for the variously sized particles. In general, a relative particle size distribution obtained by a case I system will be different from one obtained by a case II system, for accelerated particle systems.

2.1 GENERALIZED COUNTING - A STATISTICAL APPROACH

The generalized quantity which is desired to characterize the process is the distribution function based on particle flux. The total mass flow can be obtained from the distribution. This quantity is the number of particles passing through a unit area in a unit time for a unit range of particle diameters. The FOS automatically detects these particles, sizes them, and adds them to the appropriate channel. A data reduction scheme will be described which was used to determine the normalizing factors for each channel. That is, the number stored in the ith channel is representative of a particular sensing area and size. The exact area must be calculated to form the desired distribution function. To do this, the probability of a particle of a given size and at a given location on the conjugate array plane being detected and sorted into a given channel will be calculated. Once this function has been determined, average quantities (e.g., the average particle size within a channel, or the effective array length) can be calculated.

In Fig. 3 particles are shown to be moving orthogonal to the fiber array in the y direction. They are illuminated from the z direction by collimated light. The motion will carry the shadows past the array located symmetrically along the x axis. Whether or not a fiber optic module is triggered is determined only by the intensity in the shadow region and by its x position. If we assume no diffraction effects, then the shadow will be perfectly black, and geometrical considerations will adequately describe the system response.

2.2 PROBABILITY MODEL

The purpose of the probability model, which is to be developed, is to provide a method for determining the normalizing factors for each channel; this method depends on the effective array length, the sensing volume depth, and the mean particle diameter. The generality of the model allows for more complex intensity patterns in the array plane to be analyzed. Consider a particle of diameter D and position x in the array. $P_i(D, x)$ is defined as the probability of a particle of diameter D producing a count in the ith channel when located at position x. P can take on values only of 0 or 1 (no or yes). To produce a count on the ith channel the particle presence must shadow and trigger exactly i-fiber optic modules. If it does, $P = 1$; otherwise, $P = 0$. The density of particles will be assumed to be uniform over that segment of the x axis containing the array (i. e., $-X/2 < x < X/2$). P is also a function of threshold level in a manner which will be shown later.

2.3 DISTRIBUTION FUNCTION

The desired distribution function is discrete in nature (i. e., there is one value for each active sizing channel). However, one may assume that the discrete values are points taken from a continuous function.

$$f_i = \frac{d^4N}{dx\,dz\,dD\,dt}\bigg|_i$$

In the case of limited depth of field, where cutoff is provided mechanically either by physical masking or by electro-optical coincidence counting based on scattered radiation, the z-dependence can be integrated out to provide

$$f_i = \frac{d^3N}{dx\,dD\,dt}\bigg|_i \times \frac{1}{L_i}$$

where L_i = effective depth of field.

If a time average is performed with the assumption that no change in particle flux is incurred over the sample time, then

$$f_i = \frac{d^2N}{dx\,dD}\bigg|_i \times \frac{1}{L_i T}$$

where T = sample time.

5

In a similar manner, if $P_i(x, D)$ can be determined, the effective diameter and effective array width can be also obtained. This can be done by forming·

$$I_i \overset{\Delta}{=} \int P_i(x,D)dx \, dD$$

For a symmetric array of γ fibers, γ-2 of which are active,

$$I_i = 2 \sum_{\ell=0}^{\frac{(\gamma-2)b}{2\Delta x}} \sum_{m=0}^{\frac{(\gamma-2)b}{\Delta D}} P_i(x_\ell, D_m)\Delta x \Delta D$$

$$f_i = \frac{N_i}{I_i L_i T}$$

The distribution function is now reduced to measurable and calculable quantities where N_i is the stored counts in the ith channel after a period of time, T. The above equation provides the basis for a data correction computer program.

In a similar manner $\overline{D}_i$ can be calculated

$$\overline{D}_i = 2 \sum_{\ell=0}^{\frac{(\gamma-2)b}{2\Delta x}} \sum_{m=0}^{\frac{(\gamma-2)b}{\Delta D}} D_m \, P_i(x_\ell, D_m)\Delta x \Delta D / I_i$$

This is just the average size of a particle which would contribute to the counts in the ith channel. In general (see Fig. 4),

$$\overline{D}_i \approx ib = iMD_f$$

where b = fiber size in the object space, M = system magnification, D_f = fiber diameter. The effective array width is, similarly,

$$W_i = 2\Delta x \sum_{\ell=0}^{\frac{\gamma b}{2\Delta x}} P_i(x_\ell, \overline{D}_i)$$

In general this quantity is approximately (30-i)b (see Fig. 5).

6

To this point, no mention has been made of how $P_i(x, D)$ is calculated. A technique will now be developed. Consider the fiber array with a particle located at some point x as measured from the array center (Fig. 6). To determine whether a fiber will trigger or not, one need only consider the case where the number of fibers shadowed is at maximum during a particle passage. This will occur when the particle center lies on the array axis. All fibers lying totally within the particle shadow will trigger at some time during the particle transit. These fibers partially occulted must be examined in more detail.

Figure 7 illustrates the area of overlap for a round particle and a round fiber. If the area of overlap is greater than that minimum area required for triggering, the fiber will count; otherwise, it will not. This argument is strictly true only for a perfectly black shadow.

The edges of a particle are located at $d_\pm = \dfrac{D \pm 2X}{2b}$ fiber diameters. The plus sign corresponds to the edge in the positive x direction from the particle center, whereas the negative sign corresponds to the edge in the negative x direction.

The term $d_\pm$ can be expressed in terms of an integer, $J_\pm$, and a positive quantity less than unity. $d_\pm$ can be expressed as $J_\pm + \epsilon_\pm,\ 0 \leq \epsilon_\pm < 1$. The integer terms give the total number of fibers completely shadowed for an indeterminately long array, whereas the area of overlap must be calculated based on $\epsilon_\pm$ to determine if an additional one or two fibers will contribute. In practice, since the array is limited in extent, the number of fibers occulted must be checked to see if it exceeds the active array length. If it does, no counts will be registered since the end fiber reject mechanism will not allow the particle to be sized.

From geometrical considerations only, the total area of overlap (Fig. 7) is given by

$$A = A_1 + A_2 = \frac{b^2 \theta_1}{4} - \Lambda \Delta_1 + \frac{D^2 \theta_2}{4} - \Lambda \Delta_2$$

$$\theta_1 = \cos^{-1}(2\Delta_1/b)$$

$$\theta_2 = \cos^{-1}(2\Delta_2/D)$$

$$-\Delta_2 = 1/2[\epsilon - 1/2(b + D)] + \frac{D^2 - b^2}{8[\epsilon - 1/2(b + D)]}$$

$$-\Delta_1 = 1/2[\epsilon - 1/2(b + D)] + \frac{b^2 - D^2}{8[\epsilon - 1/2(b - D)]}$$

where

$$\Lambda = \sqrt{\frac{b^2}{4} - \Delta_1^2} = \sqrt{\frac{D^2}{4} - \Delta_2^2}$$

If $\epsilon_\pm$ and $d_\pm$ are substituted into the equation for A, and if b = 1, the result is area $A_\pm$.

A new variable, $K_\pm$, will be now introduced, which is defined as follows:

$$K_\pm = 0 \text{ if } \frac{A_\pm}{\pi(1)^2} \leq 1 - \text{thresh}$$

$$K_\pm = 1 \text{ if } \frac{A_\pm}{\pi(1)^2} > 1 - \text{thresh}$$

where "thresh" is the fraction of the average intensity which the instantaneous intensity must fall in order to trigger the electronics. This merely states that $K_\pm$ will take on a value of unity if threshold triggering conditions are met. Otherwise, it is zero. Now P_i can be determined.

$$P_i(x,D) = 0 \text{ if } J_+ + K_+ \text{ or } J_- + K_- > 15 \text{ or } (J_+ + J_- + J_- + K_-) \neq i$$

$$P_i(x,D) = 1 \text{ if } J_+ + K_+ \text{ and } J_- + K_- \leq 15 \text{ and } (J_+ + K_- + J_- + K_-) = i$$

P_i can now be substituted back into the equations for $\overline{D}_i$ and $\overline{W}_i$. A computer program for performing this calculation and correcting the data and a sample computer printout with accompanying explanation are shown in Tables I and II, respectively (Appendix II), in addition to the average size in the i channel and the effective array width.

The average bin size (i.e., that range of size over which particles will be sized) is in the ith channel and is given by the difference between succeeding mean channel sizes.

$$\overline{b}_i = \begin{cases} \frac{1}{2}(b + \overline{D}_2 - \overline{D}_1), & i = 1 \\ \frac{1}{2}(\overline{D}_{i+1} - D_{i-1}), & 1 < i < 30 \\ \frac{1}{2}(b + \overline{D}_{30} - \overline{D}_{29}), & i = 30 \end{cases}$$

Calculations of effective sample area, distribution function, particle flux, and particle density must be deferred until a complete discussion of the depth of field has been made.

2.4 LINEAR APPROXIMATION TO DETECTION PROBABILITY

An approximate solution will now be presented. In this case the assumption is that the array is truly linear in the sense that the fibers are b units wide in the x direction and are infinitesimal in the y direction. Therefore, an overlap of a particle will produce a reduction in intensity proportional to the fraction of the fiber covered in the x direction only (see Fig. 8).

If i fibers have been triggered, the range of particle sizes which could have been responsible may be determined by

$$D_{i\ max} = b[i + 2(1 - thresh)]$$

$$D_{i\ min} = b[i - (2\ thresh)]$$

The maximum occurs when the particle totally covers i fibers and covers just less than the amount required to trigger each of the two adjacent fibers. In a similar manner, the minimum detectable size occurs when a particle covers i fibers but covers the outermost two fibers just enough to cause them to trigger.

The size range of particles as sized in the ith channel is

$$\overline{D}_i - 1 \leq D_i \leq \overline{D}_i + 1 \text{ where } \overline{D}_i = \frac{D_{i\ max} + D_{i\ min}}{2}$$

Of course, the probability of a particle at the extreme values being counted declines to a vanishingly small value. The actual probability distribution can be obtained from the previous analysis. The total distance over the array which a particle of size D can move and trigger is given by

$$\xi_i(D) = \int_{-\infty}^{\infty} P_i(x,D)dx$$

Figure 9 shows a plot of the relative probability of triggering versus particle diameter for the linear approximation.

9

SECTION III
ELECTRO-OPTICAL REQUIREMENTS

3.1 APERTURE REQUIREMENTS

3.1.1 Minimum Numerical Aperture

The resolution of an imaging system in terms of resolvable spatial frequency is proportional to the available numerical aperture. Therefore, in system design attention must be given to the size and location of the lens so that adequate collection angles are provided.

A system must have a minimum numerical aperture (N. A.) which can be calculated based on the object geometry (Ref. 3). For a grating-like object the limit of observation is

$$|r| = 0.61 \frac{\lambda}{n \sin \theta} = \frac{0.61\lambda}{N.A.}$$

For incoherent radiation and for coherent radiation, it is

$$|r| = \frac{0.77\lambda}{n \sin \theta} = \frac{0.77\lambda}{N.A.}$$

In both cases a circular aperture is assumed. While the constant factors are somewhat arbitrary, as they depend on the form of the object, the aperture, and the sensitivity of the receptor, they are commonly used as the resolution limit.

3.1.2 Depth of Field

A particle illuminated by uniform plane radiation produces a diffraction pattern at a distance z away characterized by the particle size and the wavelength. The scaling parameter is the farfield and is given by D^2/λ.

At the distance of approximately one farfield, the intensity pattern still resembles the geometric shadow. Beyond this point diffraction effects are dominant. Therefore, the depth of field for a particle would be expected to be some constant multiple of this characteristic distance. Figure 10 shows a particle of diameter D imaged with a lateral magnification M. For small distances about the image point the longitudinal

magnification is M^2. Assuming a perfect imaging system, the disturbance at one farfield from the particle is transferred by the lens to a point approximately M^2 that distance away from the particle image. But

$$M^2\left(\frac{D^2}{\lambda}\right) = \frac{D'^2}{\lambda}$$

which is a farfield based on the image particle diameter. The introduction of a diffraction-limited lens system does not effect changes in the depth of field as sensed at the array, as the overall intensity in the shadow region decreases with z. The points of electronic cutoff will be approximately given by $z = CD^2/4\lambda$ where C is a function of the threshold. At the limits given by the above equation the intensity, on the average, will have risen above that value required to trigger a module.

By combining the numerical aperture requirement with the depth of field relationship one obtains an expression which is a measure of the adequacy of the lens system. Refer again to Fig. 10 for a simple lens system with effective lens diameter ℓ. A quantity R will be formed which is the ratio of the required numerical aperture for cutoff to the available numerical aperture. That is, for a given position, z, a particle of some size D(z) will undergo cutoff as is given by the depth-of-field relation. This particle has associated with it a minimum numerical aperture which is given by the expressions for the resolution limit, as follows:

$$R = \frac{N.A._{req}}{N.A._{avail}} = \frac{2\left(\frac{0.77}{0.61}\right)}{\ell}\left(\frac{C\lambda}{\Delta z}\right)^{\frac{1}{2}}(z_o + \Delta_z)$$

Figure 11 shows a plot of R as a function of z for $\lambda = 0.6328\ \mu$m and $z_o = 50$ cm and a lens diameter $\ell = 5$ cm. The lens in the example provides adequate numerical aperture for particles with a cutoff distance of 0.235 cm. This corresponds to a minimum resolvable particle of 48 μm. A practical limit occurs for $f/ = 1$ which would correspond to a particle diameter of 1 μm in the visible spectra.

3.2 THE OUT-OF-FOCUS OPAQUE PARTICLE

3.2.1 Intensity Distribution Calculation

A method for calculating the expected intensity distribution on the fiber optic array would allow parametric variation for system design

and analysis. Important parameters are lens-to-object distance, magnification, source wavelength, lens diameter, and, of course, particle diameter. For example, it would be of considerable interest to know in advance if a 10-μm particle could be measured and sized accurately in a tunnel where only a 5-cm lens would be available at a distance of 20 cm. It would also be desirable to know the distance over which it could be counted for an accurate depth-of-field correction.

A brief development of the equations will now be given. Figure 12 illustrates the basic geometry. This consists of a simple lens system imaging points from a distance s away from the lens onto the array plane located at a distance z = Ms, where M is the system magnification.

The particle is assumed to be an opaque disk located on the optical axis. The disk of diameter D is located a distance z away from the lens in the object field and can be specified by

$$z = s + \Delta z$$

For a typical application, Δz would be the distance from duct centerline of a uniform particle flow field monitoring system. Coordinates of the disk plane are (r_0, θ_0, z), those of the lens are $(r_1, \theta_1, 0)$, and those of the array plane are (r_2, θ_2, z'). Coherent light of unit amplitude intensity is assumed to be incident from the left.

Babinet's principle is used to determine the distribution of the light amplitude at the lens. That is, the light amplitude distribution resulting from a disk can be computed from the unperturbed distribution plus that of a hole in the following manner:

$$U_D = U_o + U_h$$

where

$$U_o = \text{wave amplitude without object}$$
$$U_h = \text{amplitude due to presence of hole}$$
$$U_D = \text{amplitude due to presence of disk}$$

On the assumption that the lens is at least a farfield from the disk, the Fraunhofer equations can be used to propagate the disturbance

caused by the disk to the lens (Ref. 4).   The disturbance then becomes

$$U_D(r_1, \theta_1) = \exp jkz \left\{ 1 - \frac{\exp (jkr_1^2/2z)}{j\lambda z} \left(\frac{D}{2}\right)^2 \left[\frac{J_i(\pi D r_1/\lambda z)}{(D r_1/2\lambda z)}\right] \right\}$$

where $k = 2\pi/\lambda$ is the propagation constant.

The disturbance is propagated through a simple lens of focal length f and diameter ℓ and results in a disturbance amplitude U_D'.

$$U_D' = \exp \left(-j \frac{kr_1^2}{2f}\right) \mathrm{circ} \left(\frac{2r_1}{\ell}\right) U_D$$

where

$$\mathrm{circ} = \begin{cases} 1, & r_1 \leq \ell/2 \\ 0, & r_1 > \ell/2 \end{cases}$$

Since the lens is less than a farfield from the array plane, the lens is the characteristic size, and the Fresnel equation must be used to propagate the disturbance through z', arriving at

$$U_2(r_2, \theta_2) = \frac{1}{j\lambda z'} \int_0^{\ell/2} \int_0^{2\pi} U_D' \exp \frac{jk}{2z'} [r_1^2 + r_2^2 - 2r_1 r_2 \cos \theta]$$

If the modified Bessel function of the zeroth order, I_0, is used, this can be simplified as follows:

$$U_2(r_2, \theta_2) = \frac{1}{j\lambda z'} \int_0^{\ell/2} U_D' \exp \left[\frac{jk}{2f} \left(r_1^2 + r_2^2\right)\right] \times I_0\left(\frac{-jkr_1 r_2}{z'}\right) \times r_1 dr_1$$

where

$$I_0 = \int_0^{2\pi} \exp [x \sin \theta] d\theta$$

$$x = -j \frac{kr_1 r_2}{z'}$$

The equation is solved by numerical integration and is tabulated in Table III.   As the photomultiplier tubes are square law detectors, the important quantity is the intensity, which is given by

$$I(r_2) = U_2 U_2^* = \left(\frac{k}{z'}\right)^2 (\mathrm{Re}^2 + \mathrm{Im}^2)$$

where Re and Im are the real and imaginary parts of the amplitude. After some manipulation they can be put in the following form:

$$Re \triangleq \int_0^{\ell/2} r_1 J_0\left(\frac{kr_2r_1}{z'}\right) \cos\left(Ar_1^2\right) dr_1 - \int_0^{\ell/2} J_i\left(\frac{kDr_1}{2z}\right) J_0\left(\frac{kr_2r_1}{z'}\right) \sin\left(Br_1^2\right) dr_1$$

$$I_m \triangleq \int_0^{\ell/2} r_1 J_0\left(\frac{kr_1r_2}{z'}\right) \sin\left(Ar_1^2\right) + \frac{D}{2}\int_0^{\ell/2} J_i\left(\frac{kDr_1}{2z}\right) J_0\left(\frac{kr_2r_1}{z'}\right) \cos\left(Br_1^2\right) dr_1$$

where

$$A \triangleq \frac{k}{2}\left(\frac{1}{z'} - \frac{1}{f}\right)$$

$$B \triangleq \frac{k}{2}\left(\frac{1}{z'} - \frac{1}{f} + \frac{1}{z}\right)$$

The intensity distribution for a sample particle geometry is given in Fig. 13. This corresponds to the image of a 20-μm particle 44 cm away from a 22-cm focal length lens of diameter 5.5 cm. The system magnification is unity; therefore, the particle is in focus. The presence of the intensity variations is a result of the finite lens diameter. The true particle radius is indicated, as well as that of 50- and 30-percent thresholds. A 30-percent threshold would undersize this particle by approximately 10 percent. The strong central intensity peak would cause certain of the fiber optic models to indicate the absence of a particle. However, as will be explained later in more detail, the gating system would still size this particle near the indicated points. Studies involving a television (TV) monitoring system illustrate this effect.

3.2.2 Television Analysis of a Particle Passage

For this study a 300-μm particle was placed on a glass disk. It was illuminated by a collimated helium-neon (He-Ne) laser beam and imaged onto a vidicon tube. The image was then displayed on a TV screen, where the image could be photographed (see Fig. 14). One of the raster lines could be selected to display the intensity profile. A series of photographs and intensity profiles was taken in sequence to simulate particle passage. For the sequence shown, the particle and array were not centered on the beam profile. While all particles within the geometric shadow are not at trigger level simultaneously, they do reach that value sometime during the particle passage.

3.3 CUTOFF LENGTH

The points along the optical axis which define the limits of particle detection are very important in determining the actual particle flux for any particular size of particle. The data reduction program includes a semiempirical equation which expresses the active length as function of particle size. For the ideal system, where the optics are not band limited and are aberration-free, a reasonable form to assume is that

$$\ell_i = \frac{C D_i^2}{2\lambda}$$

This is, of course, a statement of the scaling by the farfield relation as previously shown.

Attempts were made to determine the actual depth of field for each particle size by several means. This included using a traverse system to accurately move a particle aspirator through the focal region. The data were then used to determine average cutoff lengths as a function of size. Figure 15 shows the traverse system used, including the aspirator. The aspirator consisted of an air source consisting of 3/8-in. tubing coaxial with the 1/8-in. particle tube. Plant air at approximately 150 psig was used. A uniform supply of particles was provided by a rotating hopper/dispenser (see Fig. 16). A small 12-v d-c motor rotated a rubber-surfaced disk at approximately 1 rpm. Particles were deposited on the disk from a tube, the rate being adjusted by the clearance between the tube and the surface. A pickup was provided diametrically opposite the dispenser tube.

The experimental cutoff was obtained by dispensing equal amounts of a particle sample at various points along the optical axis. The particle distribution itself contained a broad range of sizes to produce statistically significant particle counts in each channel. The distribution can be used to obtain the average cutoff length in the following manner:

$$\bar{\ell}_i = \frac{2\Sigma \, n_i(z) \quad z_i}{\Sigma \, n_i(z)}$$

where $n_i(z)$ is the counts received in the ith channel at a position z. The sum is over-all z. The absolute value of the distance must be used; otherwise, the first moment is obtained, which is approximately zero.

15

Figure 17 shows a plot of cutoff length as a function of particle diameter. A rather drastic departure from the theoretical dependence is noted for the lower channels. Adequate numerical aperture was provided, which would rule out the effect due to bandpass limitations. The fragmentation of the image caused by beam nonuniformity may play a role. Furthermore, the particles were restricted to a region with a diameter on the order of 5 mm, and no recirculation or fanout was noted which could account for the abnormally large depth of field. That is, the indicated cutoff region is an average value, as the particle could be located ±2.5 mm about any particular position.

Electronic noise is a likely source as noise events could cause single or multiple triggers. A Poisson distribution, which statistically describes rare events, can be made to fit the lower channel counts, which is further evidence that the counts are the result of random events. By increasing the feedback at the comparator, random noise could be made to combine several single channel counts into a higher channel count. If the particles were to remain in the sample area long enough, the count would closely approximate the true particle size. This would at the same time move the cutoff point further out. Solutions to this problem will be discussed in the conclusion.

3.4 BEAM UNIFORMITY

The fiber optic system is by design relatively insensitive to illumination nonuniformities. This is a direct result of the fact that each fiber has its own photomultiplier (PM) tube and discriminator circuit which can be individually adjusted to the average intensity level at that point. Also, changes in the local light level attributable to nonuniformity of the beam coupled with vibration or some other form of beam drift are self-compensating, as the reference adjusts to slowly changing light levels. The reference level is essentially provided by filtering of the quiescent signal. Therefore, any slow changes in level will be automatically nulled out as the trigger level rises and falls with the fluctuation.

However, for the following reasons there is a requirement for a degree of beam uniformity. First, the self-compensating characteristics just outlined have limits, especially when one is dealing with low signal-to-noise ratios (S/N). Second (remembering that the beam is nonuniform), diffraction effects cause spreading of the light so that diffracted light from a point of high intensity in the object space may interfere with low-intensity

light in the image space. This effect could cause triggering on a diffraction ring instead of on the particle "edge." Such a phenomenon can be readily demonstrated. Figure 18 is a photograph of a particle in a Gaussian beam. The latitude of the film has been exceeded, giving the impression of a uniform beam. The particle center is not coincident with the illuminating beam, and the particle is out of focus. The passage of this particle across the array AA′ would probably leave many of the fiber optics located near the center untriggered, resulting in an undersized count.

If the array were located at BB′ instead, the particle passage would probably result in one oversize count as indicated by the passage of the first diffraction ring and by a count near that of the actual particle size. Figures 19 and 20 indicate intensity profiles for a particle in uniform and Gaussian illumination, respectively.

3.4.1 Uniformity Criteria for Gaussian Beam

The Gaussian beam profile is easily obtained from most lasers and possesses the unique property that it retains its Gaussian form as it propagates.

At the $1/e^2$ point of an initially collimated beam of diameter 2Ω, the intensity profile is given by the following equation (see Fig. 21):

$$I(r,z) = \left(\frac{w_o}{w}\right) I_o \exp\left(-\frac{2r^2}{w^2}\right)$$

where

$$w = w_o \left[1 + \left(\frac{\lambda z}{\pi w_o^2}\right)^2\right]^{1/2}$$

At the focal plane

$$w_o = \frac{\lambda f}{\pi \Omega}$$

where f = focal length of the lens and λ = wavelength of light (Ref. 5).

If a constraint is made on the uniformity of the illumination for variations in z such that

$$\frac{I(o,z)}{I_o} \geq a \quad \text{where} \quad a \leq 1$$

then this provides the following constraint:

$$w_o^2 \geq \left(\frac{\lambda z}{\pi}\right)\left(\frac{\alpha}{1-\alpha}\right)^{\frac{1}{2}}$$

For example, if $z = 10$ cm, $\alpha = 0.9$, and $\lambda = 0.6328 \mu$m, then the $f/ \geq 642$. If a laser which has any output diameter of 1 mm is used, the lens must have a focal length greater than 642 mm. If this were the only constraint, the lens might be avoided entirely.

Uniformity of illumination in the radial direction must also be maintained, as was discussed earlier. Demanding that the intensity not fall below a fraction, β, of the centerline intensity results in the following constraint:

$$w_o^2 \geq \frac{-2r_m^2}{\ln\beta} = \frac{-L^2}{2M^2\ln\beta}$$

where

r_m = radius of array in object space

L = length of array in object space

M = magnification of system

This may also be rewritten in terms of the effective $f/$, as before:

$$f/ \geq \frac{\pi r_m}{2\lambda}\frac{1}{(-\ln\beta)^{\frac{1}{2}}} = \frac{\pi L}{4 M\lambda}\frac{1}{(-\ln\beta)^{\frac{1}{2}}}$$

In general, the more demanding constraint will be that of radial uniformity, as the two expressions are not completely independent. Depth of field is related to particle size as the square of the particle diameter. The array width, $2r_m$, as seen in the object space, is approximately equal the maximum countable particle diameter. With these relations the ratio of w_o's can be obtained from the α and β criteria. With reasonable assumptions concerning the values of the constants involved, the relative importance of these constants can be estimated as follows:

$$\frac{w_o^2(\alpha)}{w_o^2(\beta)} = \frac{C}{\pi}\left(\frac{\alpha}{1-\alpha}\right)^{\frac{1}{2}}(-2\ln\beta)$$

18

Let C = 2.5, $\alpha = 0.9$, and $\beta = 0.9$; then

$$w_0^2(\alpha) = 0.505 \, w_0^2(\beta)$$

Because of this relation, care need be taken only in maintaining sufficient radial uniformity in the knowledge that the beam will be sufficiently uniform, axially. This is especially true if the cutoff is mechanically limited, as the maximum depth of field will never be achieved.

3.4.2 Power Requirements

In system design, the power requirement determines the laser to be used. In particularly high-loss systems, as many wind tunnel applications can be, the knowledge of the minimum power required provides a basis for calculation of actual power requirements.

By integrating the intensity equation out to some radius r, the power contained within that radius is obtained as follows:

$$P(r,o) = \int_0^r 2\pi r I(r,o) \, dr = \frac{I_m M^2}{\beta} \frac{\pi w_0^2}{2} \left(1 - \exp\left[-\frac{2r^2}{w_0^2} \right] \right)$$

where I_m is the minimum intensity level which will be encountered in the array. The total power is obtained by letting

$$\lim_{r \to \infty} P(r,o) = P_\infty = \frac{I_m M^2}{\beta} \frac{\pi w_0^2}{2} = \frac{\pi}{4} I_m \left(\frac{-L^2}{\ell n \beta} \right)$$

Tests with various β's and corresponding system magnifications substantiated the above relationship. The equation does not include the effects of wavelength change, which is contained in the expression for I_m. A knowledge of the phototube's photo-cathode characteristics can be used to predict illuminance requirements if an experimental point is obtained. For example, at 0.6328 μm, $I_m \simeq 2.7$ mw/cm^2. This requires 16.5 mw of total power for $\beta = 0.7$.

At this point a comment should be made about the use of cylindrical lenses. It is obvious that much of the power of a system designed around spherical lenses is wasted since the array is linear. Cylindrical lenses could be used to focus the light preferentially in one dimension to provide a strip of illumination at much lower total power. However, cylindrical lenses are difficult to grind and are often just slabs

of glass rod. Some applications would warrant the design of special lenses and spatial filtering, but for most installations the power loss is not prohibitive and is compensated for by ease of design and availability of components.

3.5 PARTICLE-ON-A-DISK STUDY

Another method for determining depth of field effects was to utilize a glass bead fixed to a glass disk. The disk was attached to a variable-speed electric motor, and an accurate number of revolutions could be obtained by using a strobe unit and timer.

Unfortunately, some potential problems exist with this method which cannot be totally eliminated. First is the selection of a glass disk. Since small particulates and scratches will show up as lower-channel noise, they must be minimized. The particle was attached to the glass by a weak solution of sugar and water. Second, distributions obtained in this manner are not statistically representative of even a class of particles centered about the size of interest. This is caused by repetition of the same particle, which will track through approximately the same portion of the array each revolution.

Such a study was performed using a 380-μm glass bead. Figure 22 is a composite distribution obtained by summing each channel count over the entire depth of field. This is, in effect, a simulation of a uniform distribution. From 0 to 1/4 farfields the distribution was centered on 450 μm with some counts in the first channel. The low-channel counts were attributable to dust and surface imperfections and will not be included in the composite distribution. From 1/4 farfield on out to 1-1/4 farfields the average measured size increased, finally stabilizing at an indicated size of 625 μm. This correlates with the first diffraction ring beyond the particle edge. Data were taken using a 5-mw He-Ne laser with a β of about 0.55. While this intensity ratio is not sufficient for the first diffraction ring to trigger by itself, it does drop the intensity to a point where added noise may cause false triggering. This conclusion can be further justified by the gradual increase in measured size with distance. It is this latter effect which is perhaps the most serious limitation of the FOS as it is presently designed.

SECTION IV
APPLICATIONS

4.1 ROCKET NOZZLE TEST

Tests were performed on a small rocket injector with water simulating both the fuel and the oxidizer. Normally NTO/MMH or NTO/UDMH in the ratio of about 2:1 is used. The injector was similar to those used in the Apollo Command Service Module (CSM) and Lunar Module (LM) reaction control thrusters with a design flow rate of approximately 0.35 lbm/sec. The hole pattern is shown in Fig. 23. Figure 24 illustrates the detailed dimensions of a simple hole doublet.

This particular injector was chosen since data existed concerning the particle distribution as measured using an in-line holocamera (Ref. 6 and Fig. 25). Water was injected at 75 psig into both the oxidizer and fuel manifolds. This resulted in an average discharge velocity of 2.7×10^3 cm/sec at the nozzle face.

Data were taken 6.1 cm downstream of the rocket face and 2.54 cm off the axis. Masking tubes provided mechanical aperturing of the spray. An upstream slit width of 7.49 cm was maintained while the downstream side was cut away to eliminate entrained water from settling on the optics. Figure 26 shows the masking tubes. Splitter rings were turned on the tubes to help prevent droplets from flowing along the surface and off the ends into the sampling area. Some breakup of droplets caused by the edge was expected. Since the slit width was approximately 10 times the depth of field of the smallest particle, the effect of breakup on the result should be small. The end effects were therefore assumed to be negligible.

The bin size was selected as 25 μm, and a 30-percent threshold was used. The illumination source was a 5-mw He-Ne laser with a beam diameter at the exit of about 0.65 mm at the $1/e^2$ point. Beam divergence was 1.7 milliradians. This provided an illumination spot diameter at the sample area of approximately 1.50 mm. This is approximately twice the array image or maximum measurable particle size.

Table II summarizes the results of the FOS data taken at the same conditions as the holography test. An explanation of the symbols and format follows the table. For comparison a constant velocity for all

particles was assumed which was applied to the measured particle flux to obtain the densities. An average density of 24.56/cm^3 was measured over a period of 7.44 sec as compared with 33 ± 5.2/cm^3 at one instant in time for the holography (as based on 27 particles). The particle flux as measured by the FOS is shown in Fig. 27. The log of the flux is plotted, as there usually is a larger number of particles in the small channels. However, these particles contribute little to the overall volumetric average diameter. Also shown are the geometric sizes of the injector holes (see Fig. 24).

A Nukiyama-Tanasawa plot of both the FOS and the holography data was made in which the two are compared (see Fig. 28 and Ref. 7). The Nukiyama-Tanasawa expression derived for jet impingement, following Ingebo, is given by

$$\log F = \log \frac{\Delta R}{(b)D^5} = -1.7 \frac{D}{D_{30}} + \log \left[(3.915)^6 \Big/ D_{30} \Big/ 120 \right]$$

where

$$\Delta R = \frac{\text{Volume contribution of size D particles}}{\text{Total volume of all particles}},$$

$$b = \text{bin size, and}$$

$$D_{30} = \text{volume mean diameter.}$$

In general, D_{mp} is given by

$$D_{m_p} = \left[\frac{\Sigma n_i \, D_i^{\,m}}{\Sigma n_i \, D_i^{\,p}} \right]^{p/m}$$

A plot of log F versus D has a slope given by

$$D_{30} = -1.7 / \text{Slope}$$

In Fig. 28 a volumetric mean diameter was calculated directly from both FOS and holographic data. This was used to generate the lines passing through the data.

The data were corrected for two reasons. First, although the same bin size was used, the method of sorting the particles by the FOS was basically different from the manual reduction method used with the holographic analysis. An approximate 1/2-bin shift was introduced which

which was adjusted at the lower end. Second, the probability for counting the large particles is very low. In fact, if a total of 400 particles is recorded, as was the case for the hologram, the probability of not counting a particle in the higher channels becomes greater than the probability of obtaining a count. Therefore, the data obtained by the FOS was again modified to exclude these points for comparison purposes only.

Agreement is in general good; however, severe deviations are noted at both the high and low ends of the range. As this effect is common to both sets of data, it will appear that the irregularity is a function of the fluid-particle dynamics rather than a system error. The time average D_{30} = 293.4 μm of the FOS was based on 16,061 points. The spatial average D_{30} = 270 μm of the holographic system was based on 400 points. The difference is approximately 8.3 percent or 0.936 b.

Plume profiles of various quantities can also be readily obtained. With the aperture tubes in place a scan was made over the radius of the plume at a distance of 23.5 cm downstream. The aperture width was fixed at 1.19 cm, thereby sampling an area of approximately 2.5 mm^2. Figure 29 shows plots of diameter as a function of plume radius. Note the decrease in size as the edge of the plume is reached. Hologram shadowgraphs near the face indicate this trend. Figure 30 plots particle flux and density as a function of radius. This, too, clearly falls off in a monotonic fashion. Particle flux measurements are exact insofar as this is the measured quantity. However, the inferred density should be taken with some caution, as the discharge velocity at the face was used in its calculation. A decrease in particle velocity with increasing radius and downstream distance would be expected. This velocity, in general, is size dependent. An independent velocity measurement could be used to produce densities if desired.

4.2 DUST EROSION TUNNEL

The FOS was installed in the PWT Dust Erosion Tunnel to investigate system performance at high velocities of reasonably well-known particles.

The flow is obtained from a continuous operation arc-heated wind tunnel equipped to conduct erosion tests of materials under high-velocity and high-enthalpy conditions (see Fig. 31). The tunnel, which has a

maximum run time of five minutes, is capable of using particles from 50 to 1000 μm with velocities up to 6500 ft/sec depending on size. It utilizes high-pressure air heated in a 5-MW arc heater.

Particles are injected upstream of the nozzle throat of a low-expansion-rate, hypersonic nozzle, where they are aerodynamically accelerated. The test section consists of a test cabin and a multiple-mount model injection system (see Fig. 32). An exhaust connection is provided through a diffuser to the Engine Test Facility (ETF) exhaust plant. The installation is shown in Fig. 33.

4.3 MICROSCOPE COMPARISON

A comparison of grits prepared for use in the Dust Erosion Tunnel (DET) was made. Nominal 650-μm grit was sized by the FOS utilizing the aspirator and dispenser. A sample was also sized by conventional microscope techniques. Figure 34 shows a direct comparison of the two distributions. Both distributions show a very large number of particles in the 5- to 100-μm range in addition to those greater than 650 μm. The FOS did not include particles below 16 μm, which may account for the lower number of particles registered in this bin. Figure 35 shows the same distributions normalized to the total number of particles in each distribution.

A notable departure is found in the 200- to 650-μm region. This is a direct result of the use of magnesium oxide particles and the method used in characterizing the diameter. Figure 36 is a photo-micrograph of the particles. Note the irregular nature of the crystaline particles and the presence of small fragmentation particles. The FOS sizing is based on a projected length. Random orientation of the particles, as verified by double-pulsed holography, produces the wide variation in measured sizes. The microscope count was based on the maximum linear dimension. The average ratio of maximum-to-minimum linear dimension is 1.4. Furthermore, a close inspection under the microscope indicates that, due to their geometry, the particulates orient themselves preferentially on the surfaces. In general, they seek a stable orientation, thereby introducing a bias in the distribution toward the larger indicated size.

SECTION V
APPARATUS

5.1 THEORY OF OPERATION

The fiber optics system has already been described in some detail. It consists of an imaging system of sufficient numerical aperture to pass at least the first minimum of the smallest particle pattern. This portion must be specifically designed for particular application. Next is the fiber array, extending for 0.844 cm and composed of thirty-two 264-μm fiber optics. The electronic detection system consists of 32 PM modules, an input sensor strobe module, and a size encoder (see Fig. 37). External power supplies provide -6, +12, and +5 volts and an adjustable high-voltage supply for the photomultipliers. An additional clock and memory inhibit were added to provide timed input for rate determination.

5.2 PHOTOMULTIPLIER DETECTION MODULE

As shown in Fig. 37, light is channeled from the linear array to the corresponding 931A PM tubes located on printed circuit boards in a modular chassis rack. Interlocking, light baffled tubes allow the boards to be removed for servicing and still allow a close interface between fiber ends and the PM tubes. The current from the tubes, nominally 100 ma, is connected to the input of a 702 current-to-voltage converter producing a signal level of about 3 volts. The output of the 702 is sampled and is inverted by a 741 operational amplifier to provide a reference voltage. A low-pass input filter allows power supply ripple and 1/F noise to pass to later null with similar noise in the signal.

The low-pass 3-db point can be increased up to almost 0.5 MHz, where the 741 begins to roll off. The signal and reference outputs are summed at the input of a 710 comparator. The comparator changes state if the signal drops below the predetermined threshold. Some feedback is provided for clean crossover. This is supplied by voltage division of the positive output and typically is 50 mv.

The comparator output is inverted by a 7402 NOR inverter, the output of which is through a pair of diodes (IN914). One diode from each of the 32 modules leads to a common output to form an expandable NAND function to sense the particle transit. The other diode output is inverted and sets a latch. The $\overline{Q}$-latch output connects to the size determination encoder, while the Q output drives a lamp through a 2N3643 transistor for static tests of the individual boards. The latches are reset by pulses from the input sensor and strobe generator logic module.

5.3 INPUT SENSOR AND STROBE GENERATOR

The common outputs from the PM board modules form the NAND Gate input (Fig. 37), which is at a logic '0' during particle shadow transit. A DT932 quad-input OR gate provides a logic '1' for the transit time. This output is inverted, and the trailing edge of the pulse sets an S-R flip-flop (7474). The leading edge of the 7474 output triggers a 9601 one-shot, providing a delay to allow for crossover noise. The output triggers a second one-shot to provide a strobe pulse. The last one-shot provides a reset pulse for the PM module latches after a suitable delay. The 7474 output also is used to provide an inhibit pulse back to the PM modules to prevent a second particle from entering until the first has been processed.

5.4 SIZE DETERMINATION ENCODER

The size encoder (Fig. 37) provides a parallel binary representation of the memory address to the particle data handling system. The outputs from the PM modules are summed in five adding levels by a combination of full adders. The basic circuitry is standard. However, in addition to the 30 size channels possible are the conditions of single and reject and oversize or double-end reject. These channels are 0 and 31, respectively, and correspond to triggering of one or both of the end modules during a particle transit.

5.5 PARTICLE DATA SYSTEM

Up to this point, the electronic processing has been described in some detail. The data handling system, however, contributes little to the information-gathering process and merely provides data storage, display, and handling capabilities and will be only briefly discussed (see Fig. 38).

The data handling system provides storage for 32 channels of information, 30 of which correspond to size data; the remaining two are used for end-reject data as previously described. Each of these channels may be read out by the Nixie tube display or on the cathode ray tube (CRT). They are sequentially updated at the frame rate. (One full frame is equivalent to a complete reading of the 32 memory units.) The memory may be reset manually or automatically by selection of a frame reset rate. Memory transfer is controlled manually, but may be controlled by an external source. This simply controls the

acceptance of data into the memory units. In conjunction with the memory transfer switch an external scaler-timer is enabled to give elapsed counting time.

The CRT display can be scaled by up to a factor of 100, calibrated, and positioned from the panel. An analog signal is also provided, which is a direct result of the digital-to-analog conversion necessary for the vertical sweep.

BCD output is also provided, together with a print command pulse, to drive a printer. The channel number and the counts in that channel are printed out sequentially at a rate which can be determined through hardwiring to the timing oscillator.

5.6 REJECT PROCESSOR AND GATED STROBE

Information from the particle-sizing system includes five binary lines for particle sizes, two lines for end fibers, and a strobe line (Fig. 37). The logic for acceptance or rejection of the size determination is performed within the particle data system. It is at this point that a valid strobe pulse is generated to allow the size determination to address a memory unit. Assuming that no end fibers have been occulted, the BCD input will be used to address the appropriate memory and the strobe pulse will index the count contained by one. An invalid or reject strobe, if generated by one or both fibers being occulted, will cause the appropriate address, 0 or 31, and index it by one.

Additional gating is provided to drive counters to record separately right- or left-end fiber rejects. This information might be useful for highly nonuniform flows.

SECTION VI
CONCLUDING REMARKS

The FOS offers a versatile means of particle sizing in flow-field situations. It has real-time capability and is compatible with most digital data handling systems. Data reduction programs are straightforward and proven. Through the use of curve fits and prerun calibration a minimal amount of computing capability is required for an on-line monitoring system.

The major drawback of the system is that caused by poor electronic depth-of-field cutoff. This effect can be reduced by means of mechanical aperturing as was done in the water spray tests. Other approaches exist which could reduce the effects of noise coupled with the out-of-focus particle transits. A crossed beam coincidence would reduce these spurious effects.

The crossed beam approach would rely on the coincidence of scattered light and particle shadow transit. The volume would be defined by that volume about the object plane of the imaging system in common with an off-axis collection system and an apertured photomultiplier tube. Such a system would allow localized measurements to be made within flow fields whose extent along the optical axis is on the order of or less than the cutoff distance.

REFERENCES

1. Knollenberg, R. G. "The Optical Array: An Alternative to Scattering or Extinction for Airborne Particle Size Determination." Journal of Applied Meteorology, Vol. 9, No. 1 (February, 1970), pp. 86-103.

2. Trollinger, J. D. and Belz, R. A. "Holography in Dust Erosion Facilities." AEDC-TR-73-160, September 1973.

3. Born, Max and Wolf, Emil. Principles of Optics. Permagon Press, New York, 1964 (Second Edition).

4. Goodman, J. W. Introduction to Fourier Optics. McGraw-Hill, San Francisco, 1968.

5. Bloom, A. L. Gas Lasers. John Wiley and Sons, Inc., New York, 1968.

6. Belz, R. A. and Dougherty, N. S., Jr. "Holography of Liquid Reacting Sprays." Proceedings of the Symposium on Engineering Applications of Holography, February 16, 1972. Advance Research Project Agency of the Department of Defense. Conducted by TRW Systems Group, Redondo Beach, California.

7. Ingebo, R. D. "Vaporization Rates and Drag Coefficients for Isooctane Sprays in Turbulent Air Streams." NACA TN 3265, October 1954.

APPENDIXES
I. ILLUSTRATIONS
II. TABLES
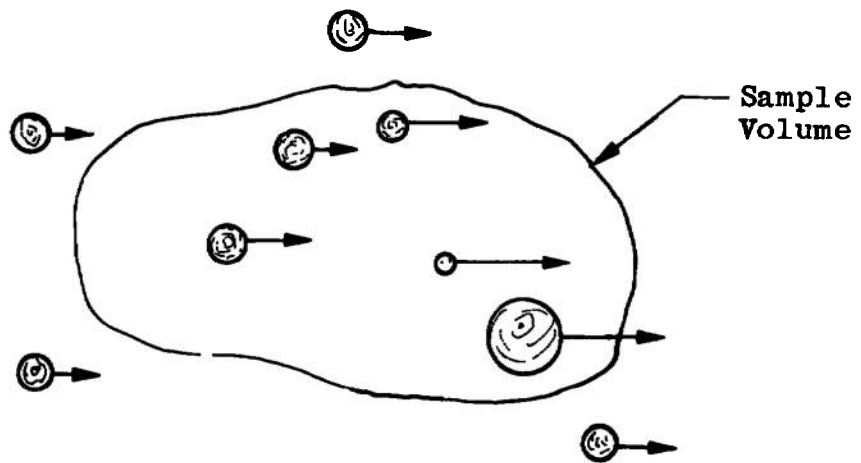
Fig. 1 Sample Volume
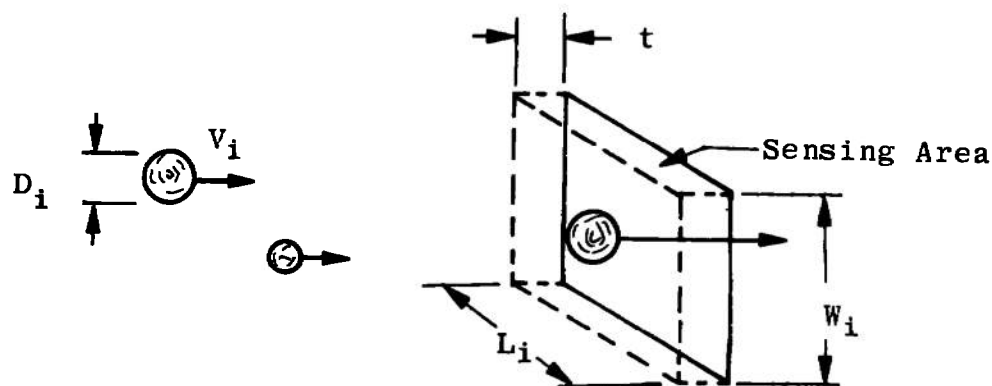
Fig. 2 Sample Area
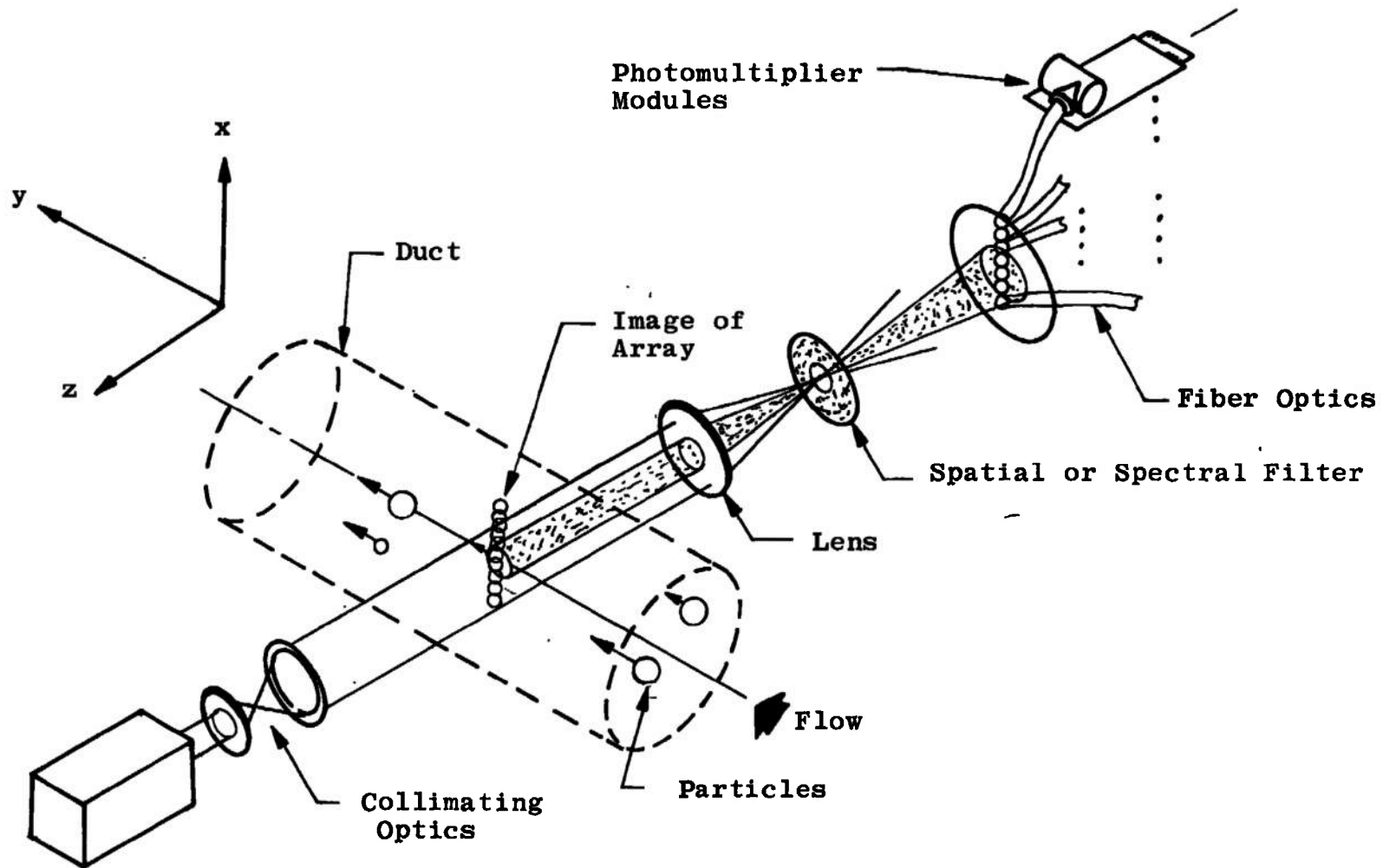
Fig. 3 Typical Fiber Optics System
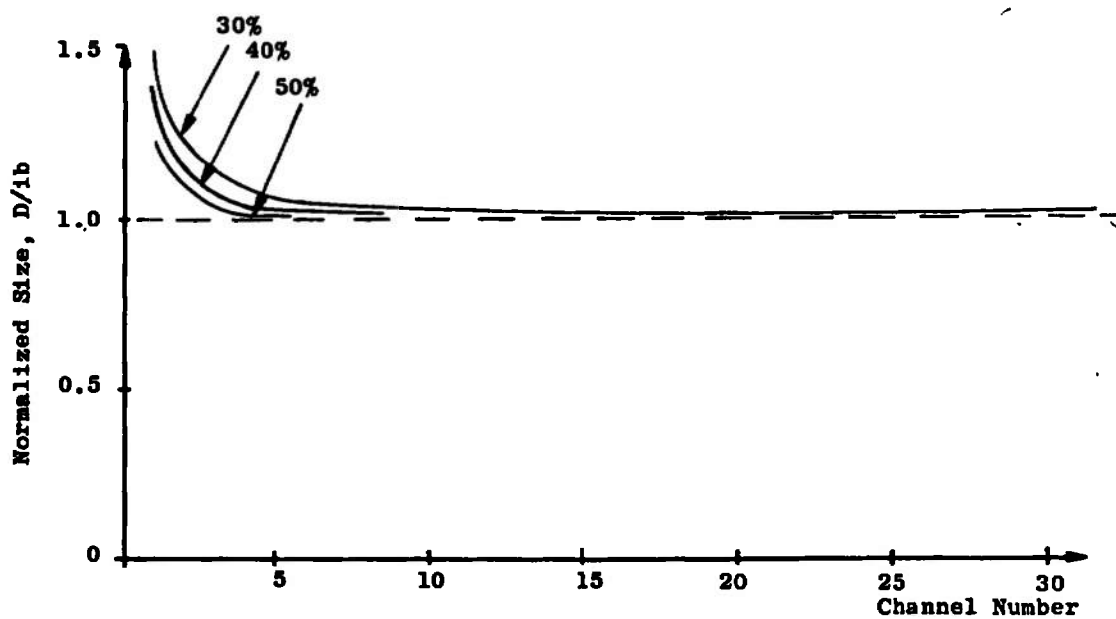
Fig. 4 Normalized Mean Size versus Channel for Various Threshold Values
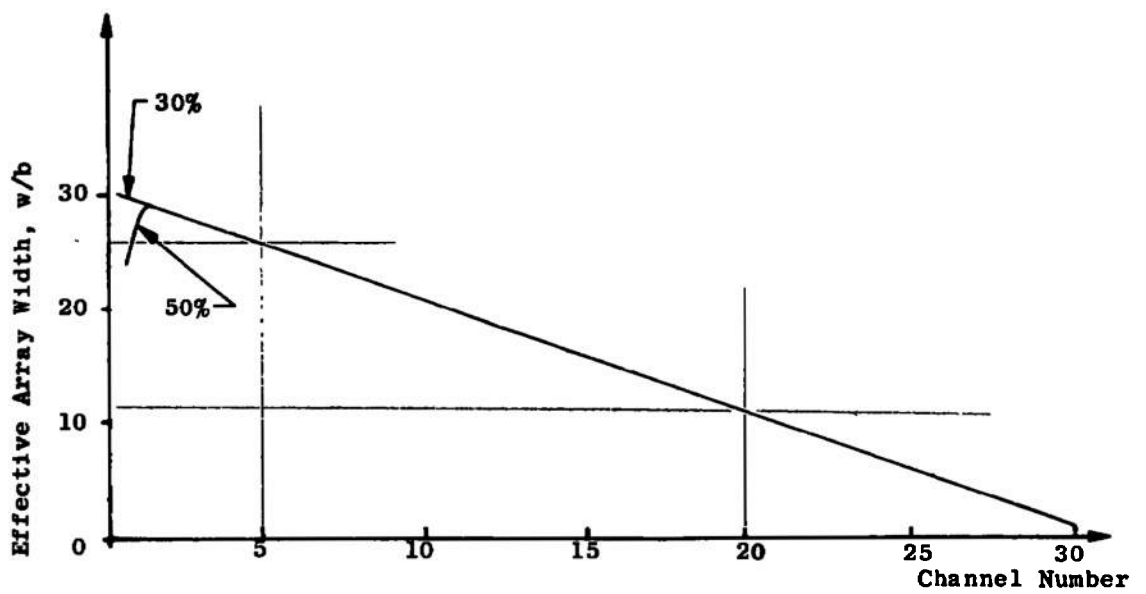
Fig. 5 Normalized Array Width versus Channel Number for Various Thresholds
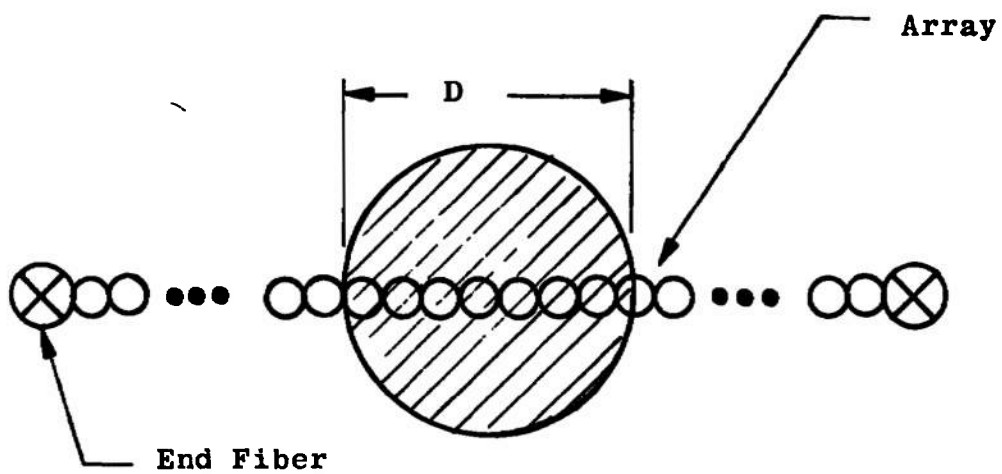
Fig. 6 In-Focus Particle on Array
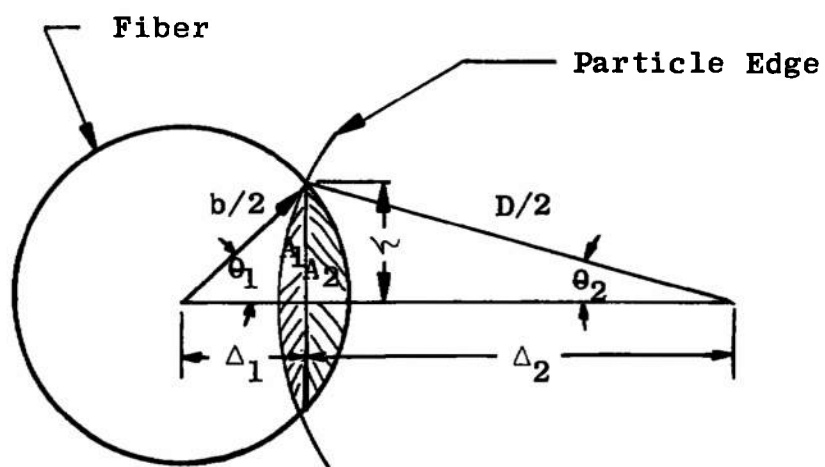
Fig. 7 Fiber/Shadow Overlap
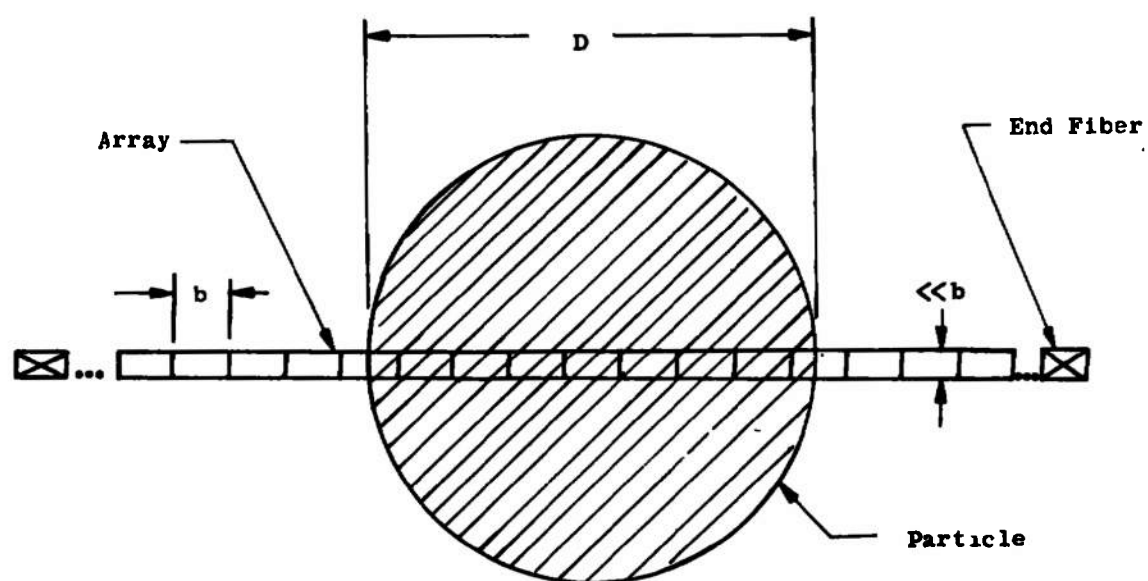
Fig. 8 Particle on Linear Fiber Array
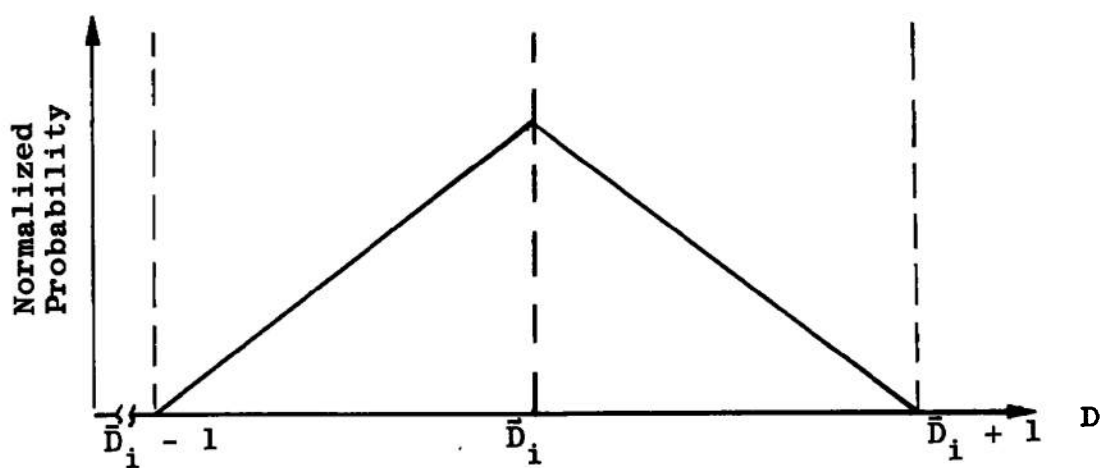
Fig. 9 Probability of Triggering in ith Channel versus D
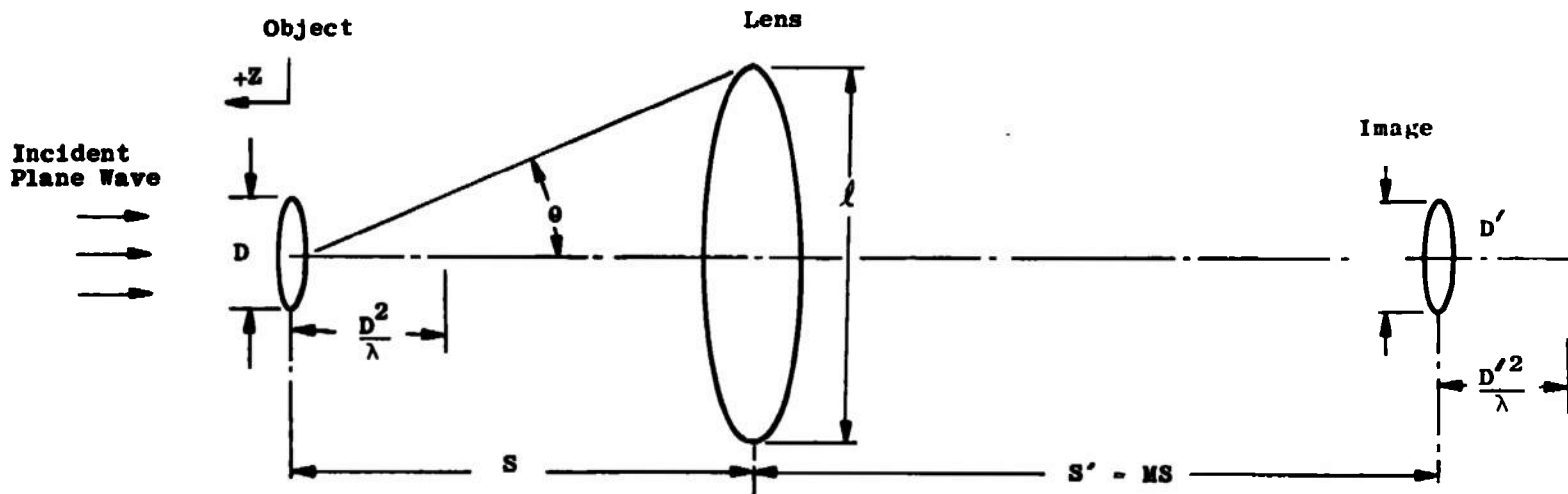
Fig. 10 Depth of Field
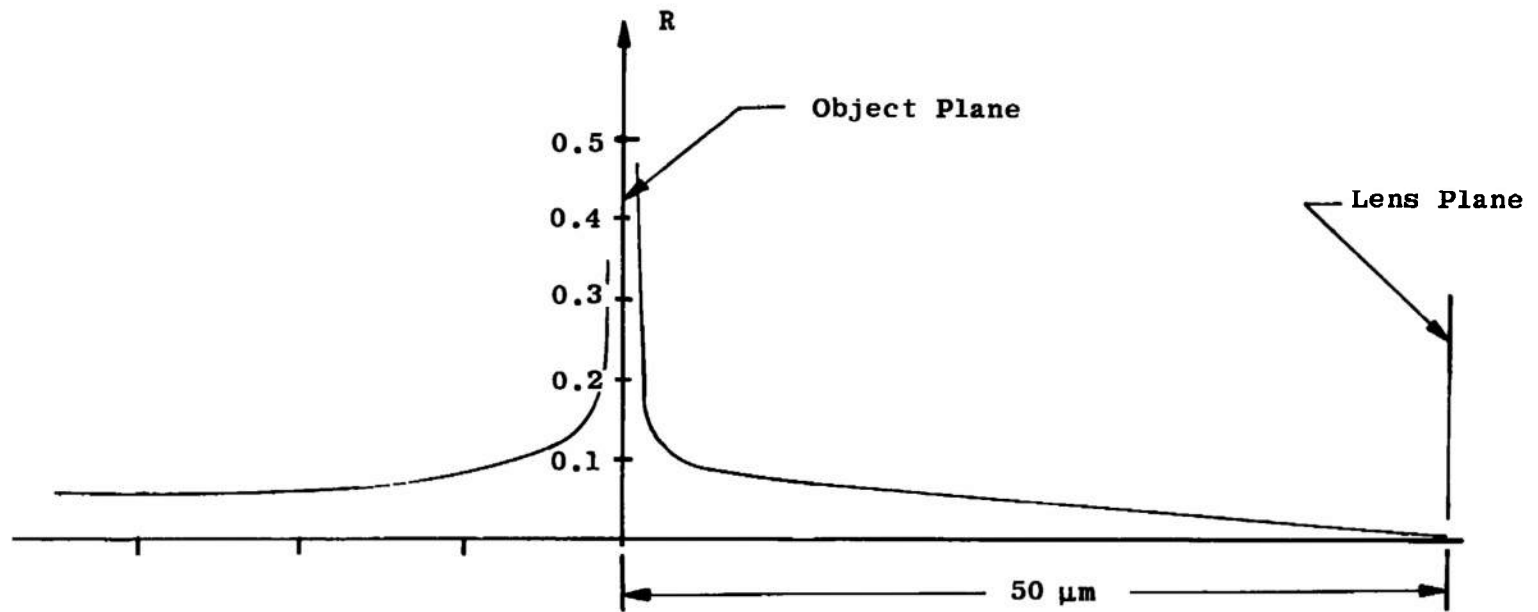
Fig. 11 Ratio of Numerical Apertures versus Position

Disk

(r_0, θ_0)

Object Plane

Lens

(r_1, θ_1)

Array Plane

(r_2, θ_2)

Δ

s

z

z = MS
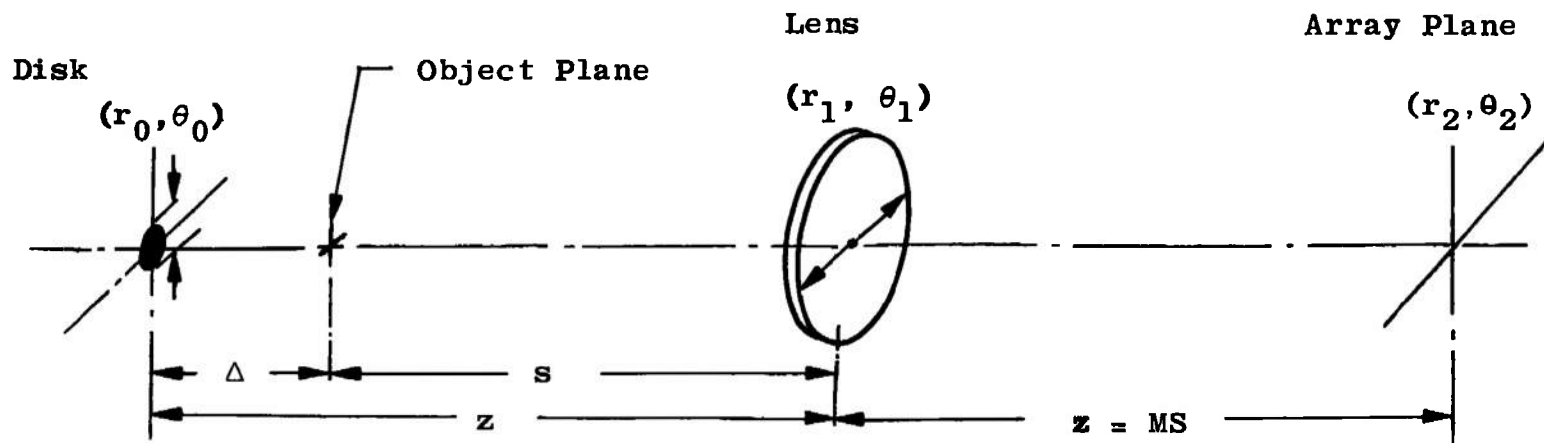
Fig. 12 Opaque Particle Geometry
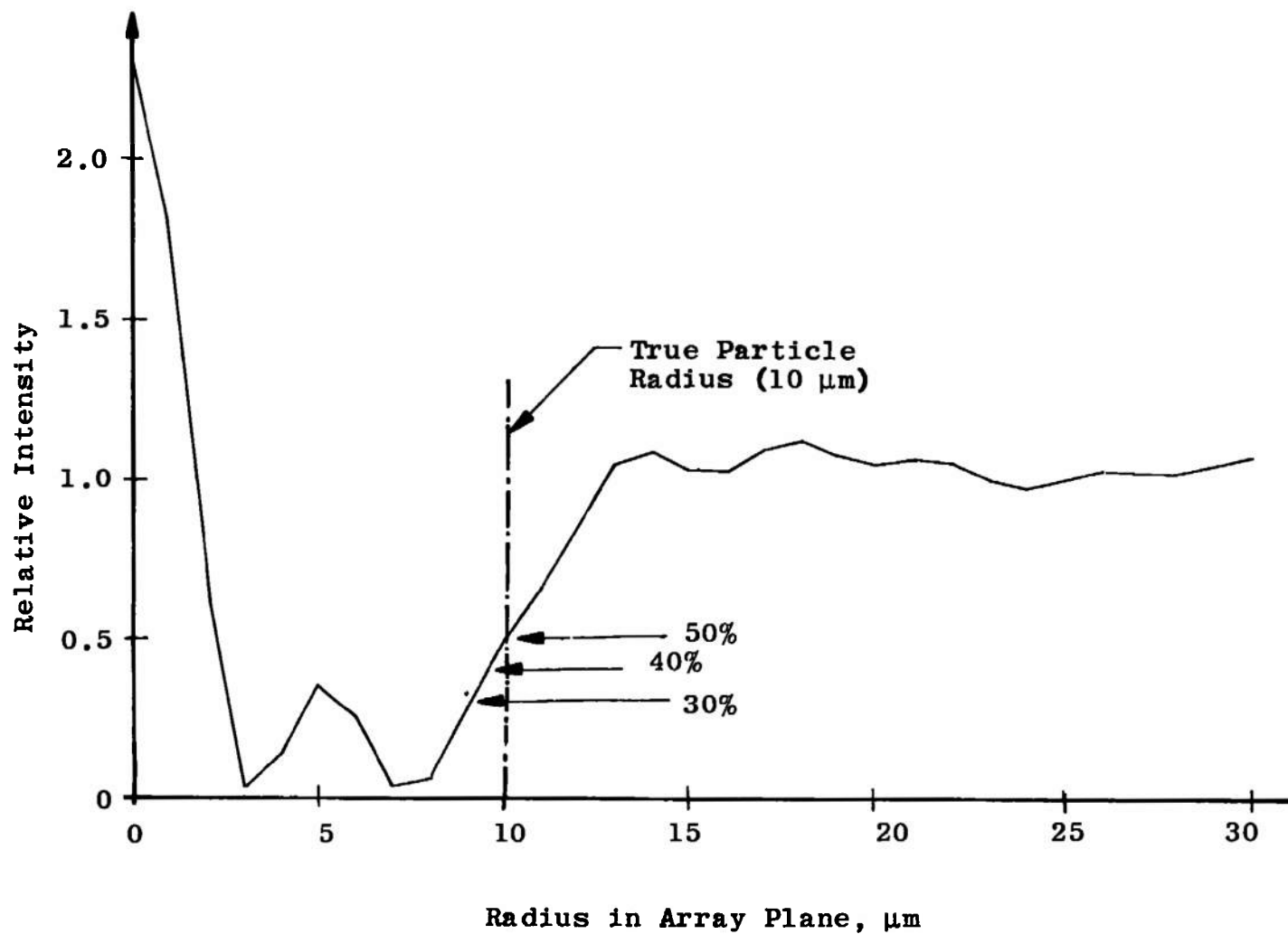
Fig. 13 Intensity Distribution of a 20-μm Particle
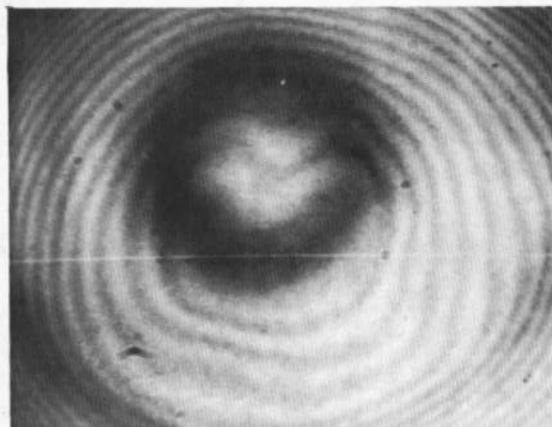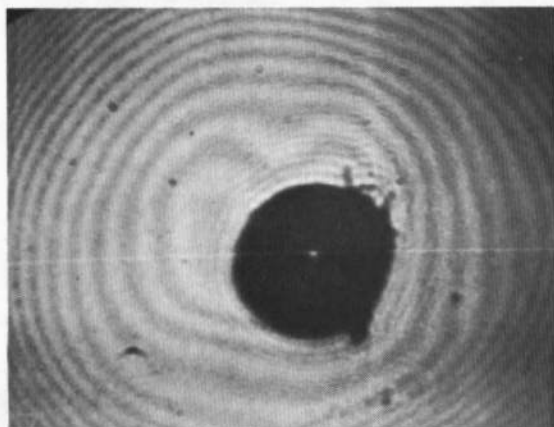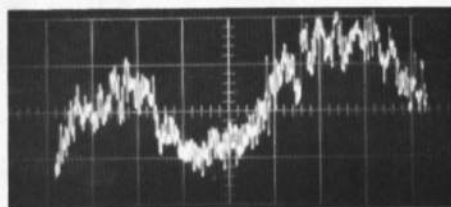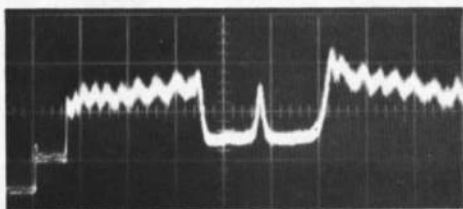
a. In-Focus Center

b. Out-of-Focus Edge
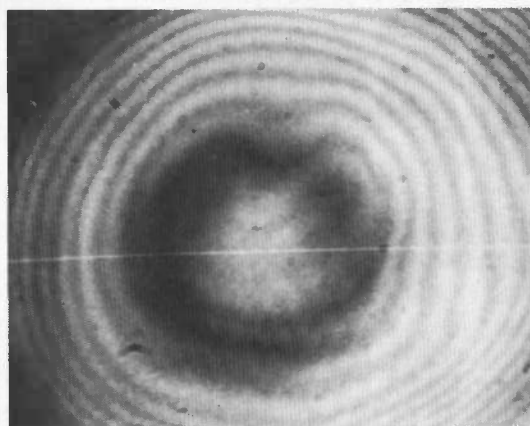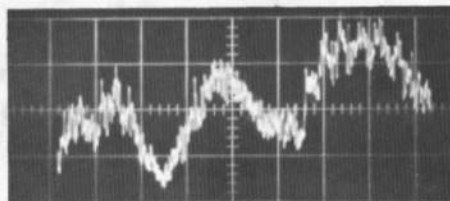
c. Out-of-Focus Center
Fig. 14 Intensity Profiles of 300-μm Particle
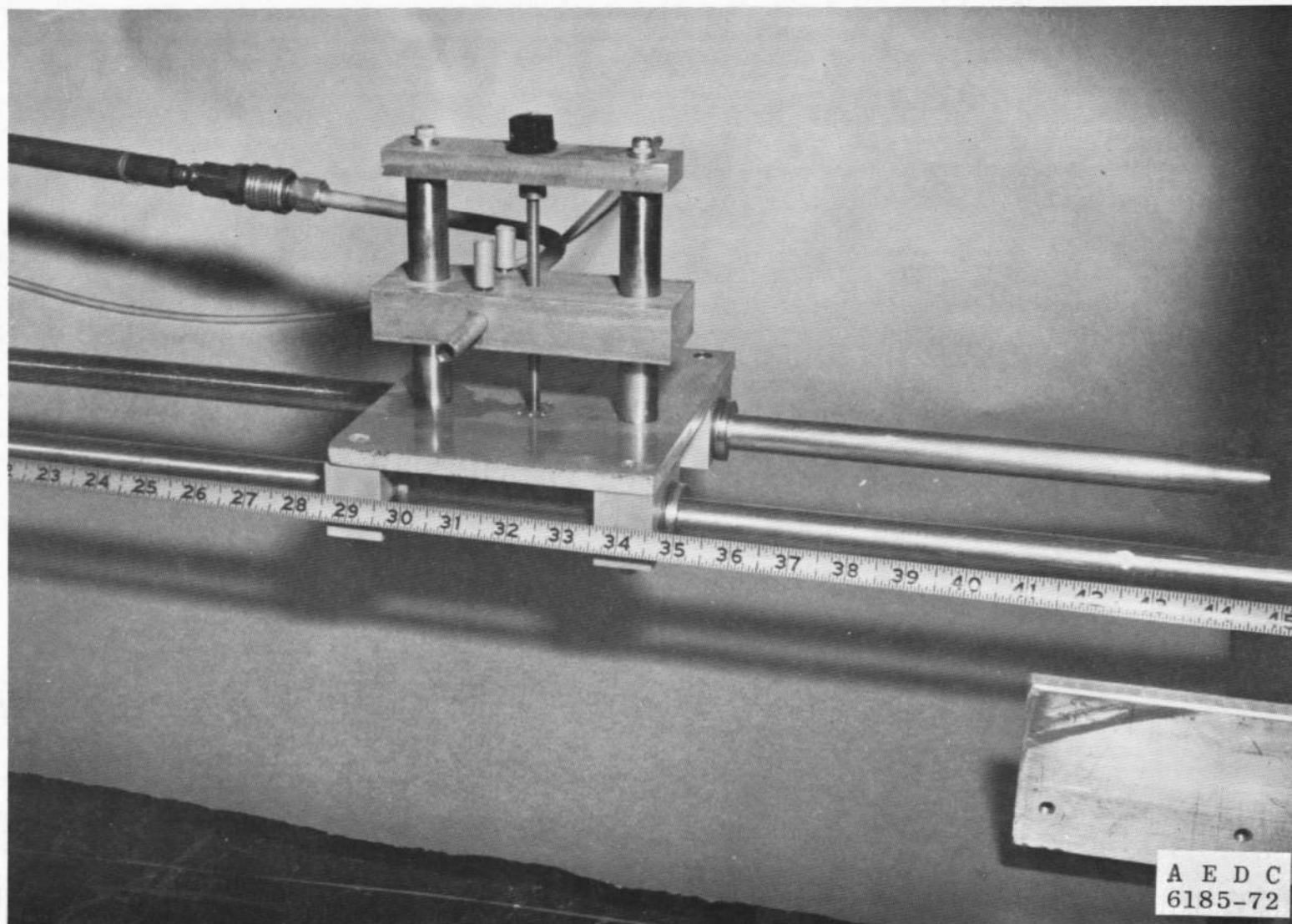
Fig. 15 Traverse System
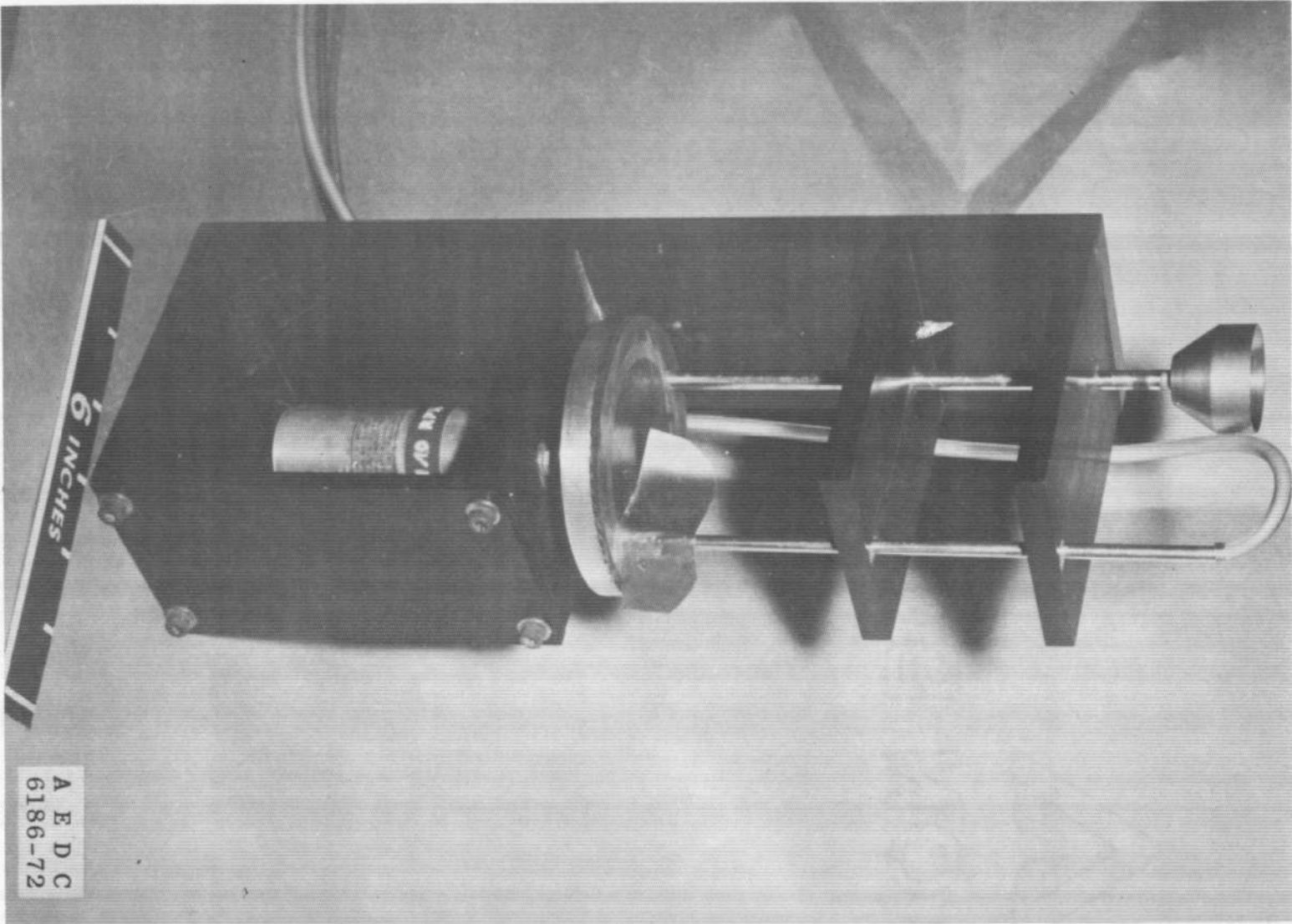
Fig. 16 Particle Dispenser
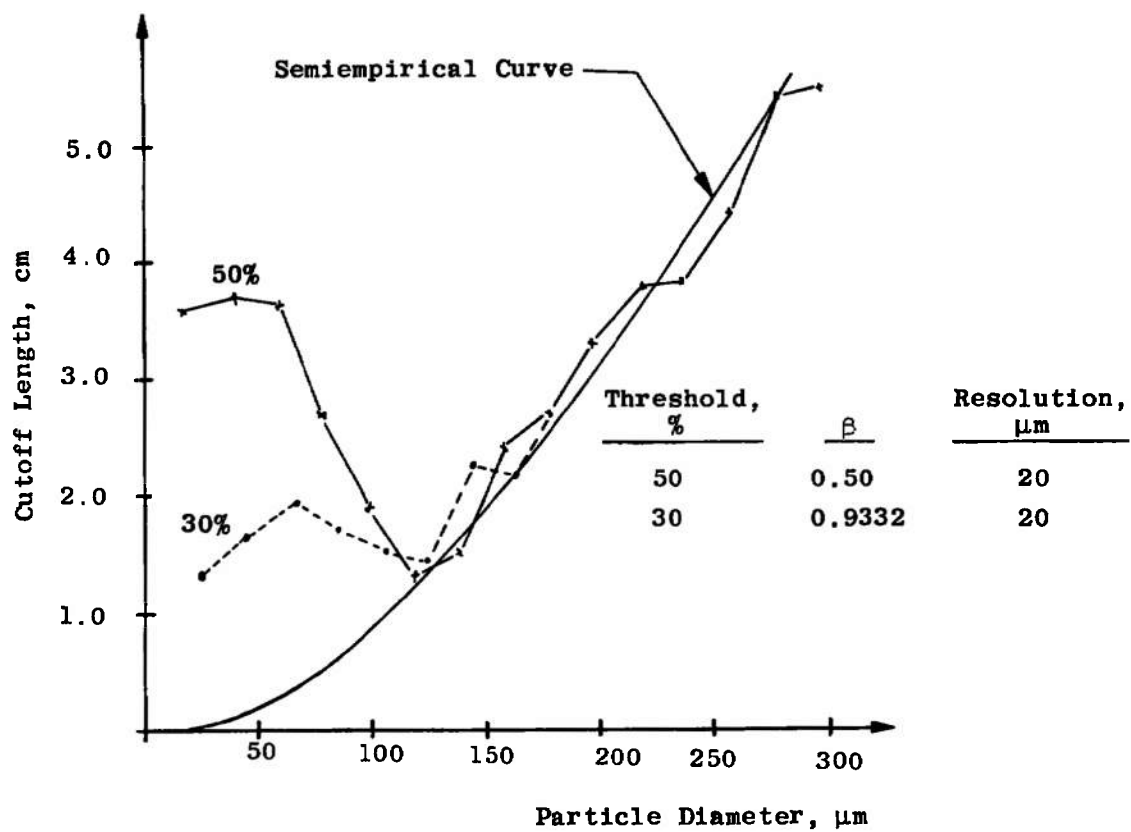
Fig. 17 Cutoff Length versus Particle Diameter
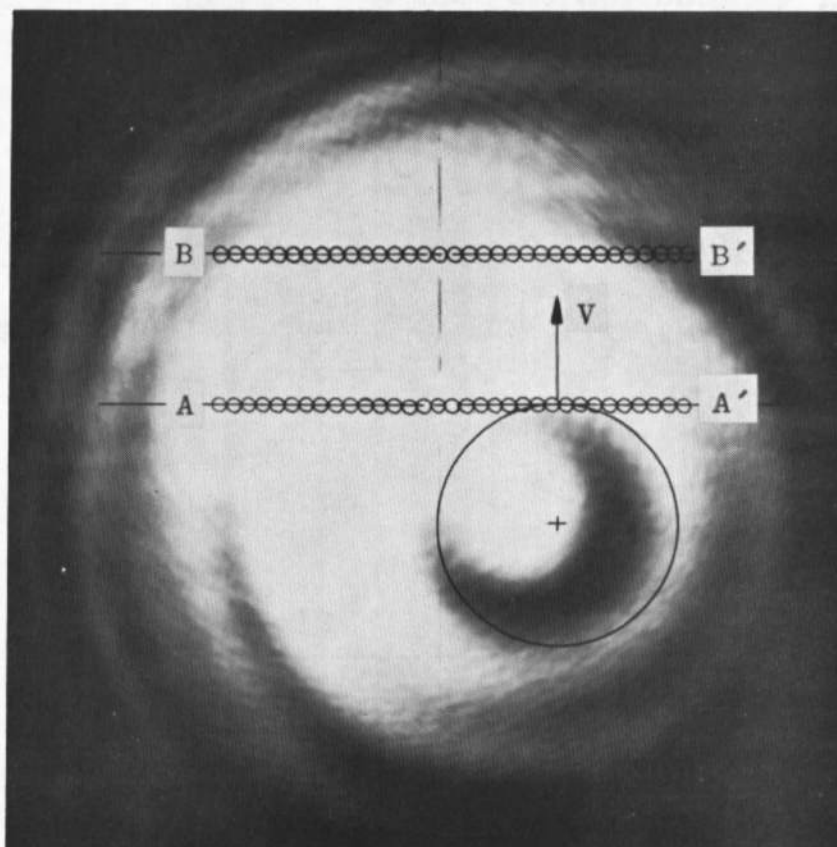
Fig. 18 Particle in Gaussian Beam
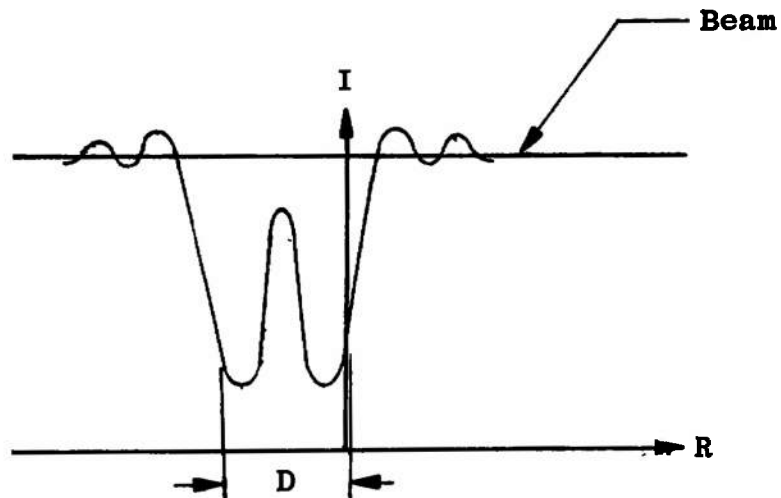
Fig. 19 Schematic of Particle in Uniform Beam
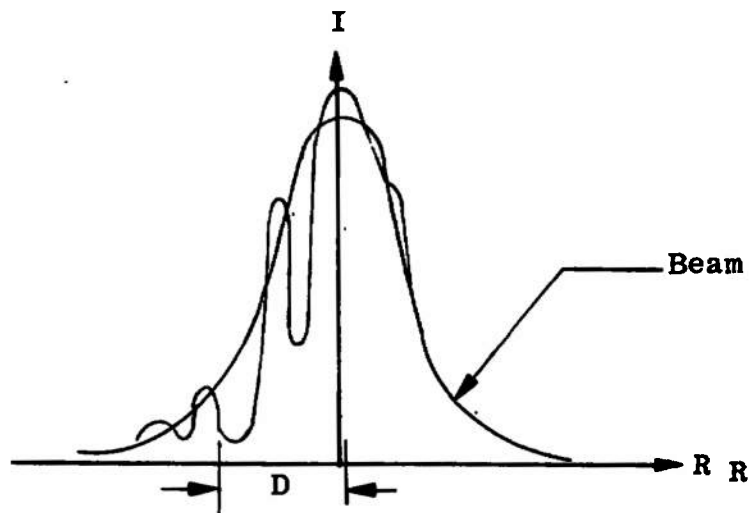
Fig. 20 Schematic of Particle in Gaussian Beam

49
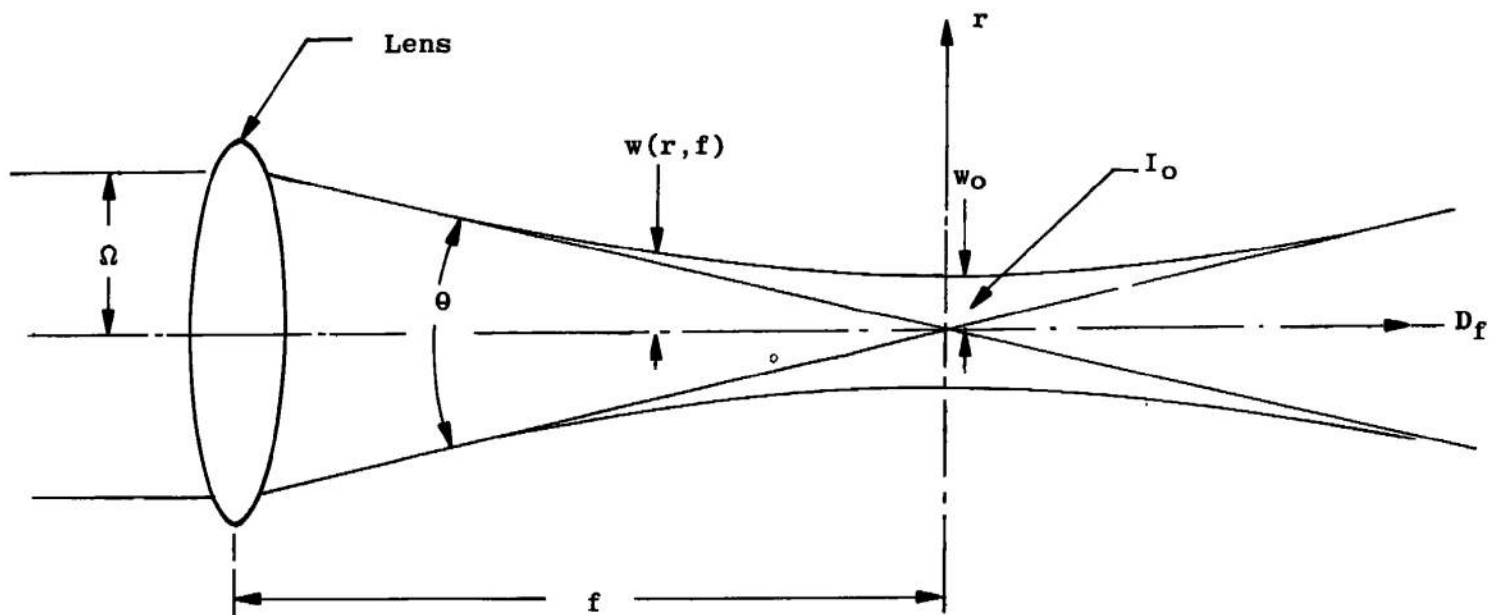
Fig. 21 Focused Gaussian Beam
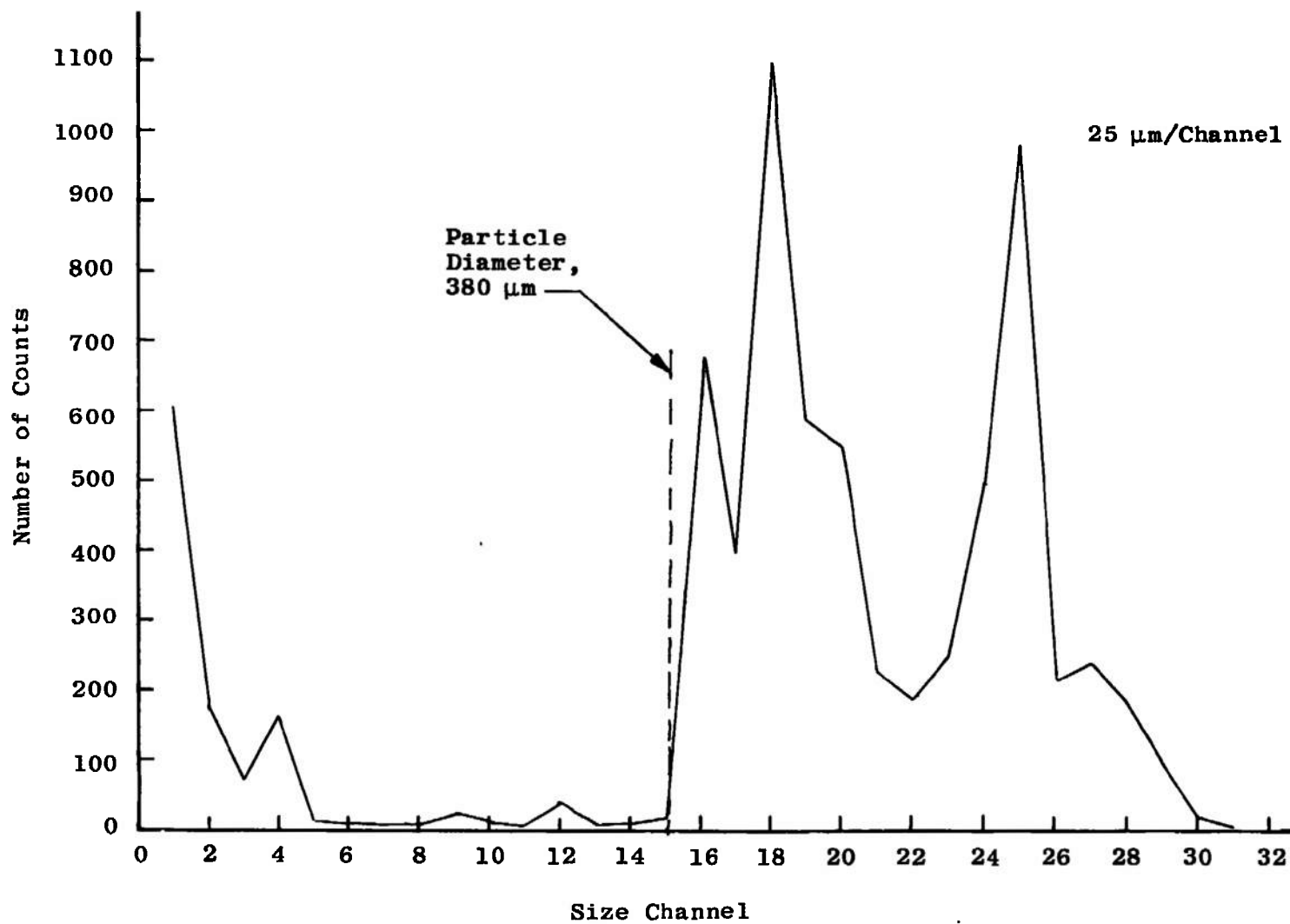
Fig. 22 Composite Distribution of Particle on Disk
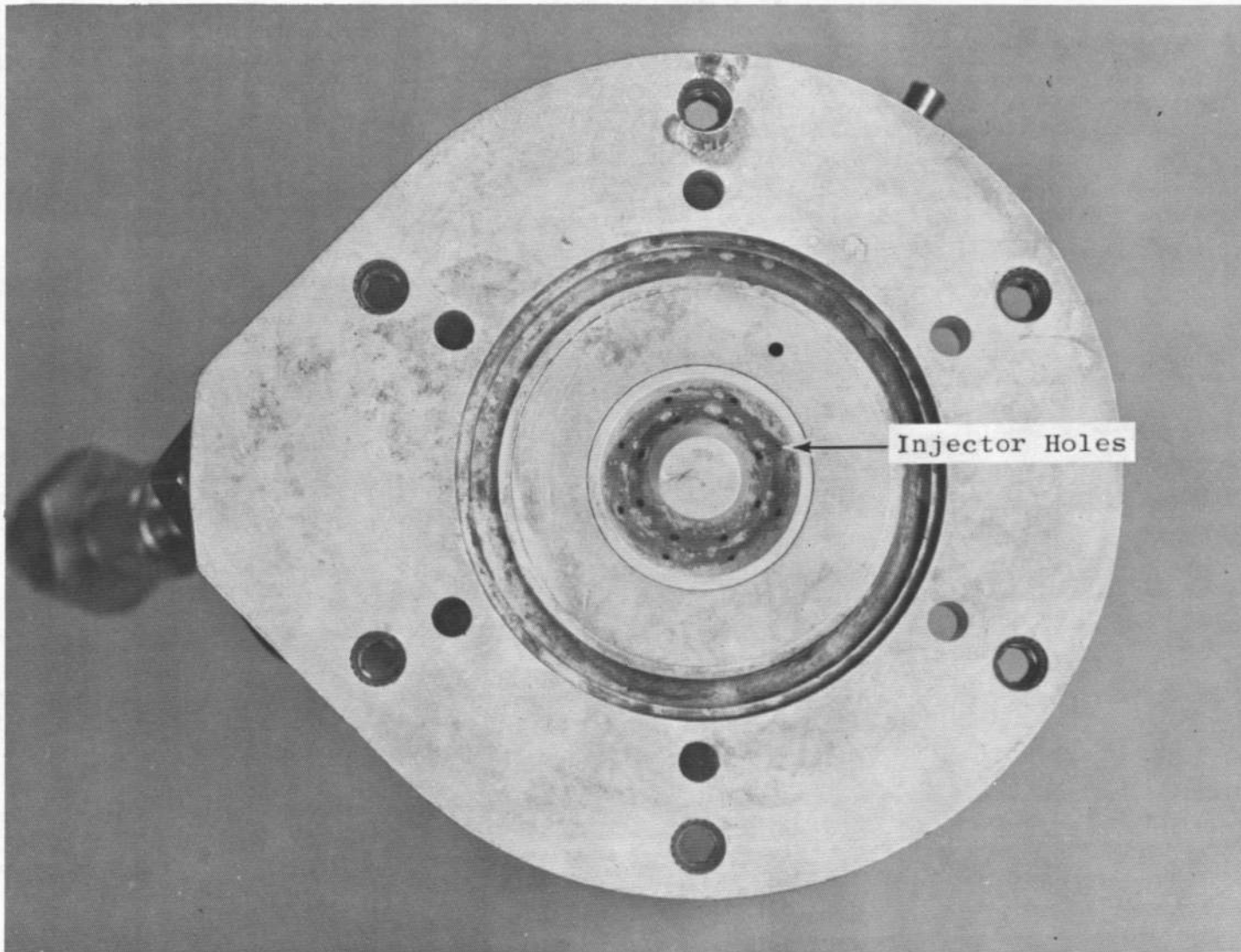
Injector Holes

Fig. 23 Rocket Injector Hole Pattern
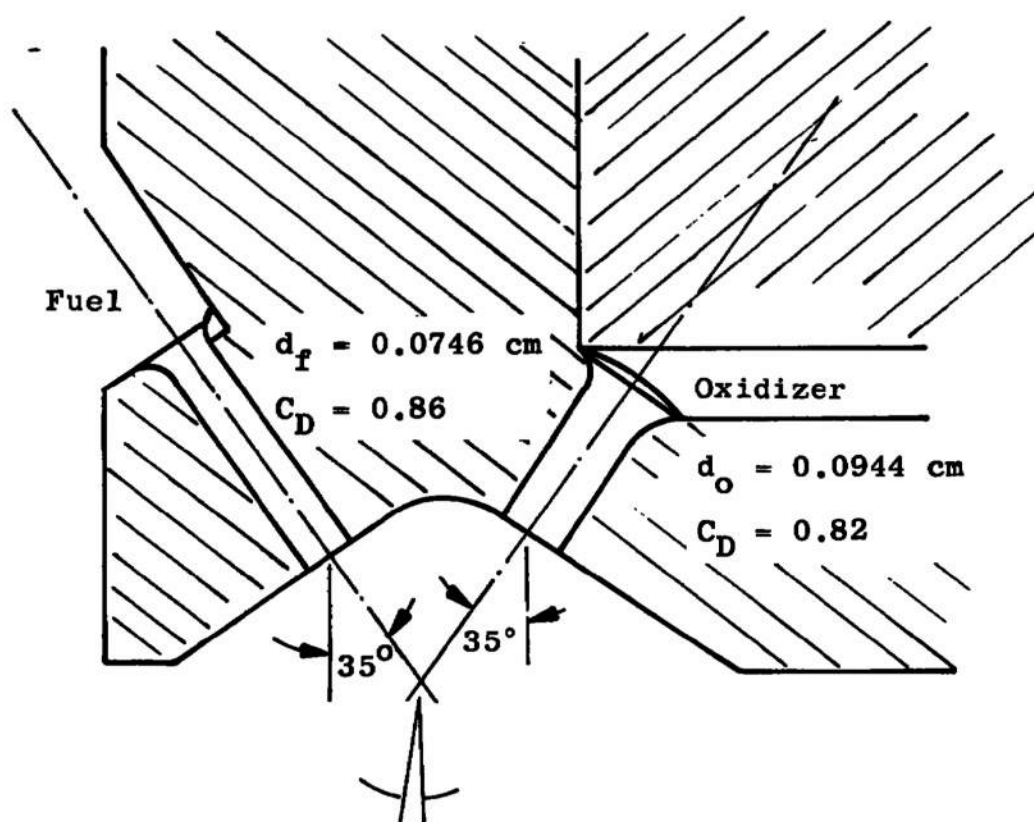
Fig. 24 Nozzle Hole Doublet

Fig. 25 Rocket Injector Spray Test
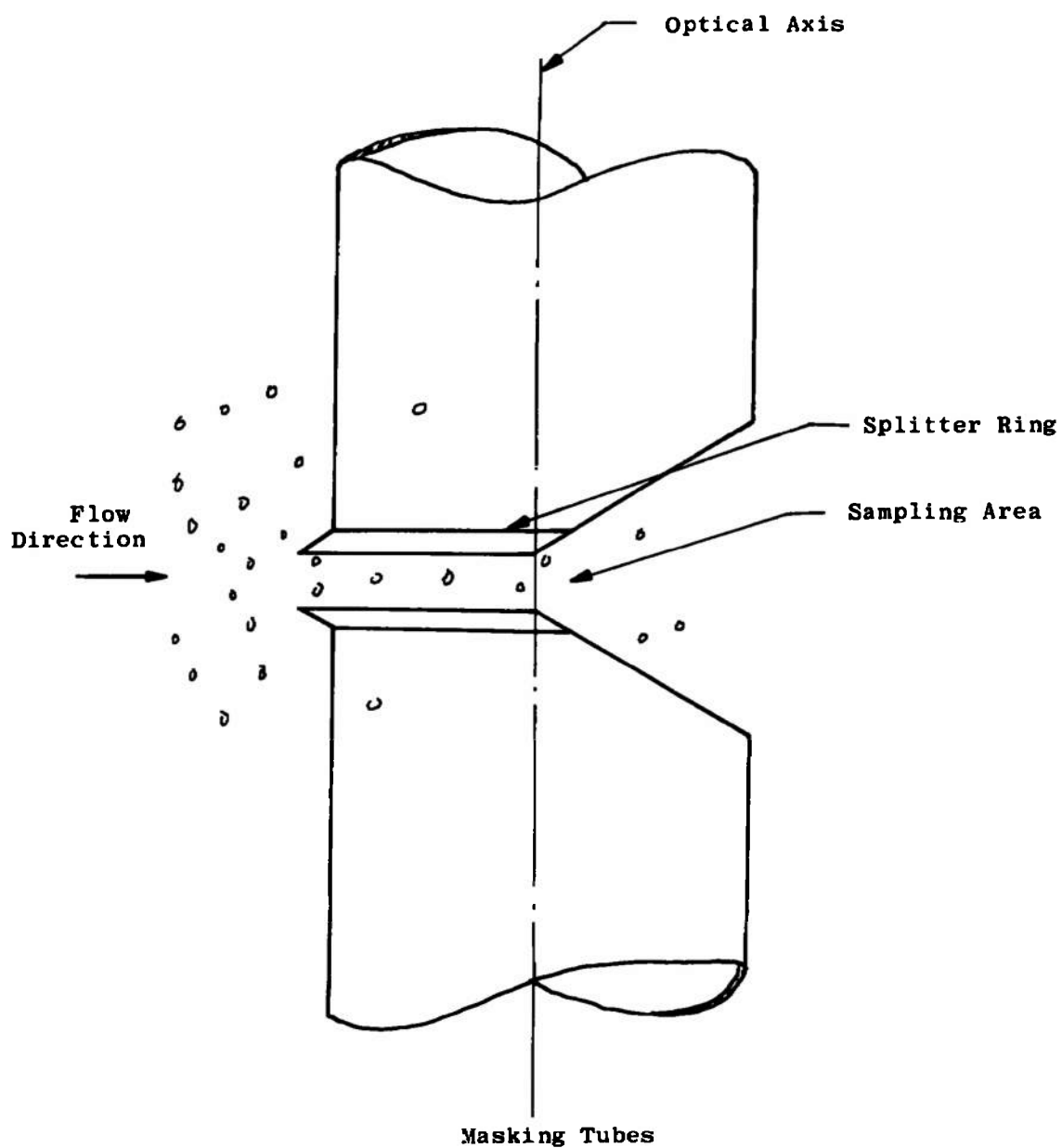
Fig. 26 Masking Tubes
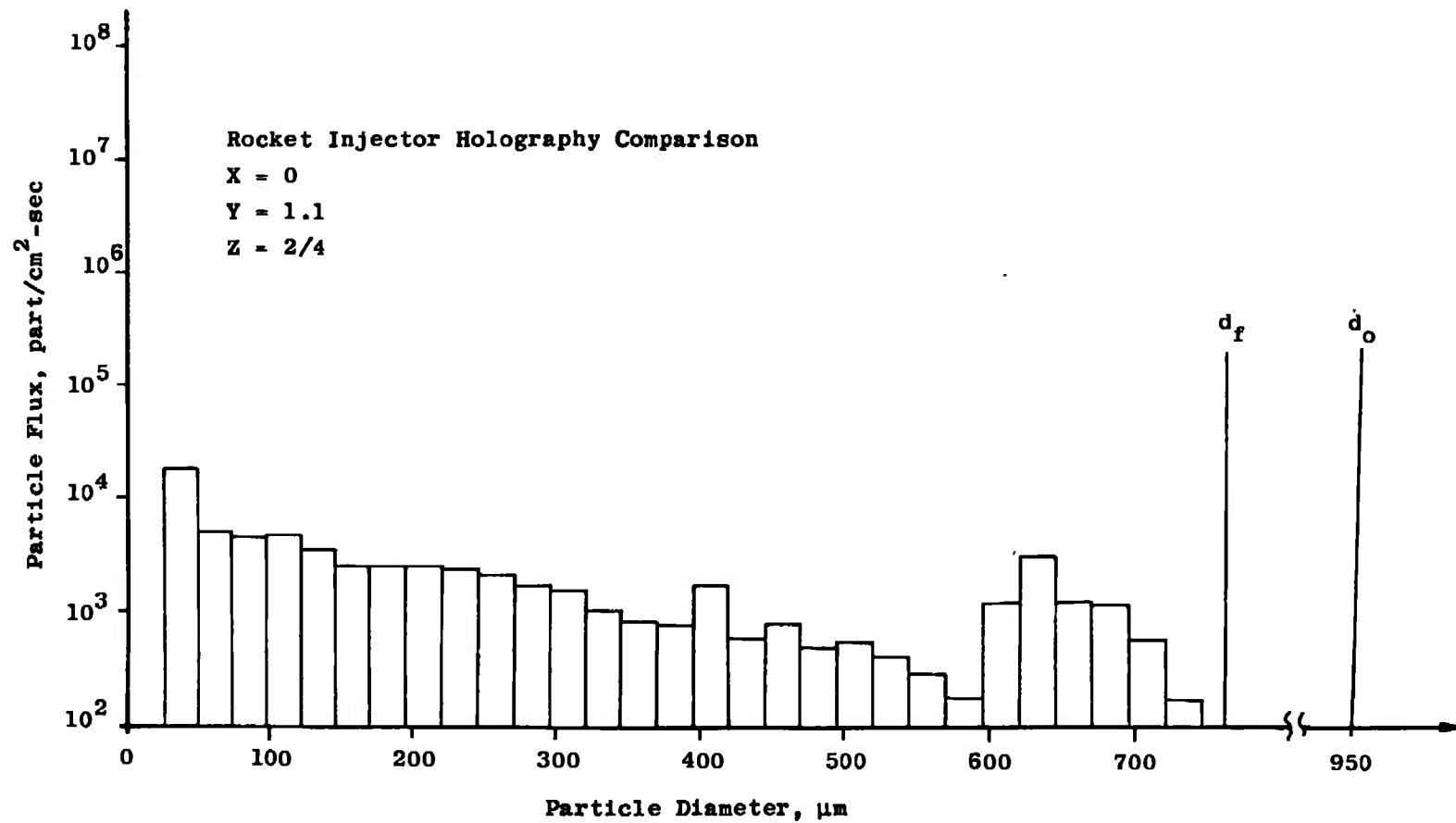
Fig. 27 Particle Flux versus Size
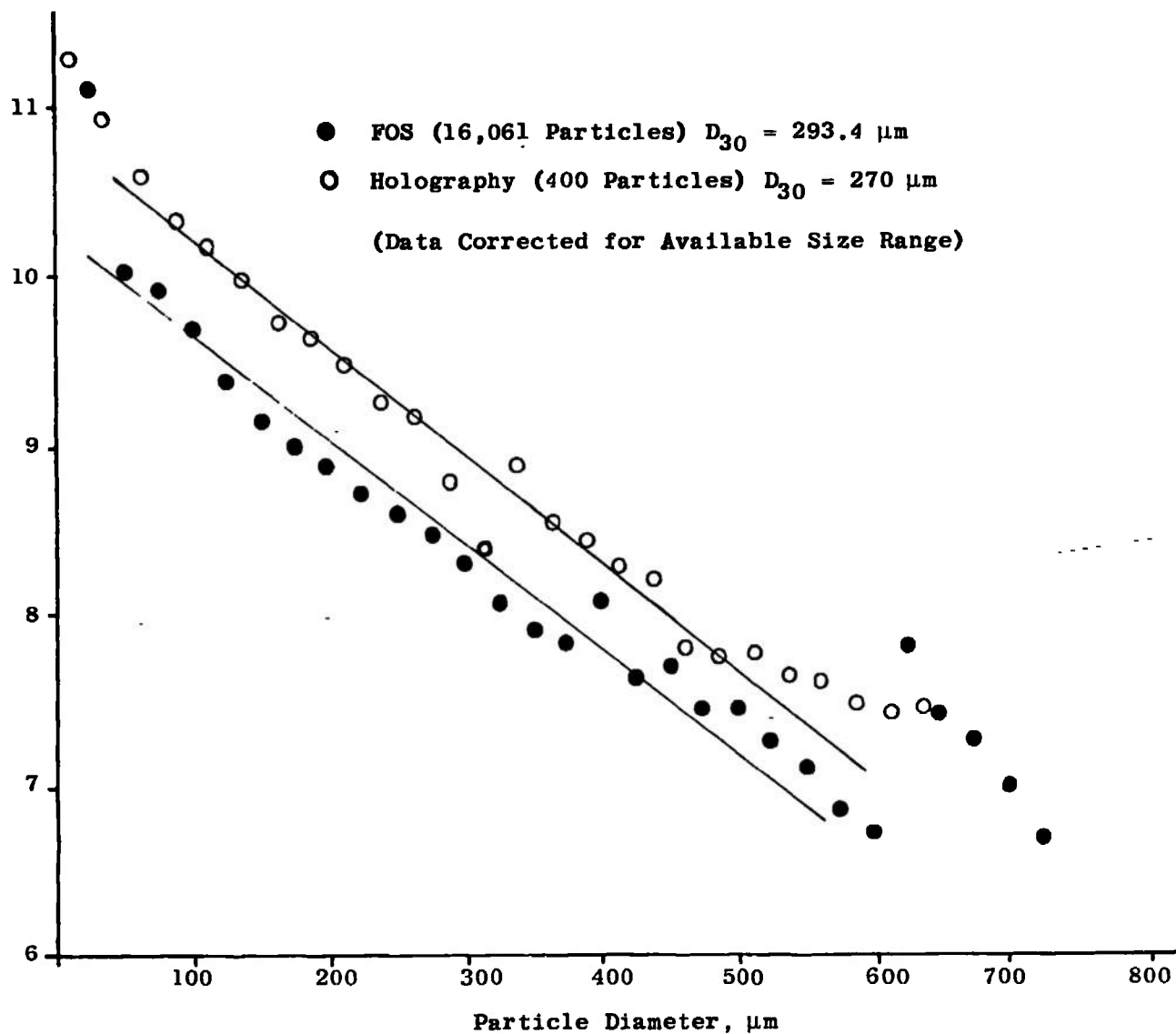
Fig. 28 Nukiyama-Tanasawa Analysis
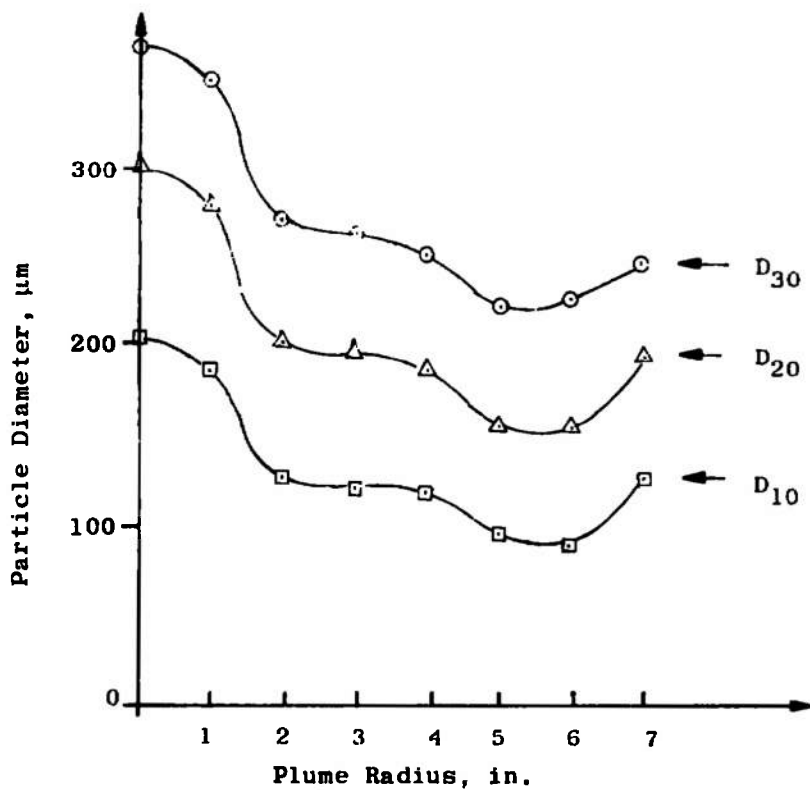
Fig. 29 Mean Diameter versus Radius
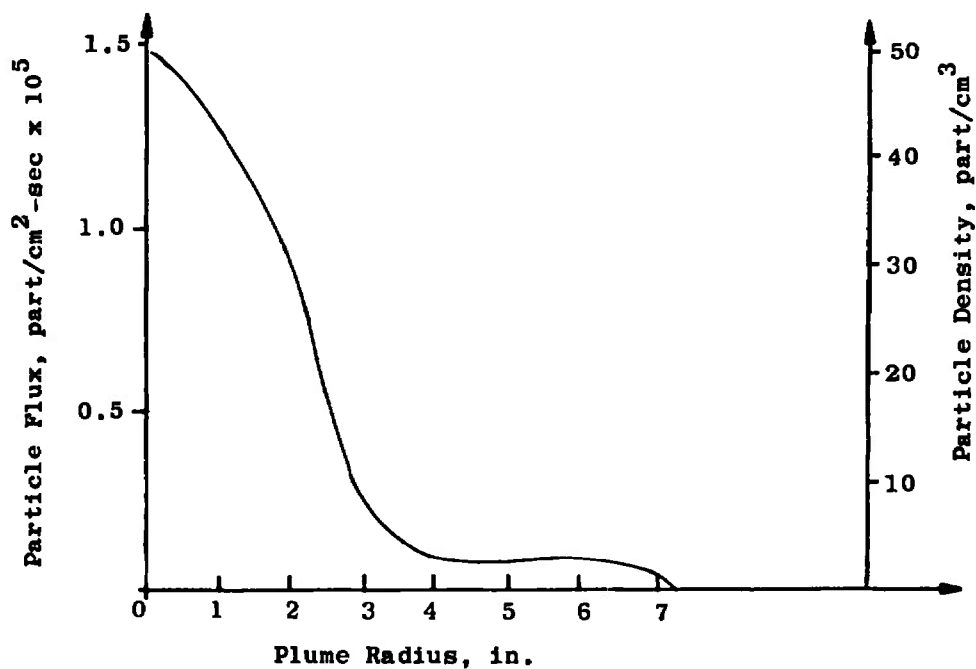
Fig. 30 Particle Flux and Density versus Radius

Dispenser
Adaptor

Arc
Heater

15 ft   Exit 15.xx in.

9/16 in.

1° - 2° divergent angle

8 in.

Laser

Arc Heater

Test Cabin

Nozzle

Diffuser

Fiber Optics System

Subsonic Cone

ETF Exhaust
Duct

Isolation Valve
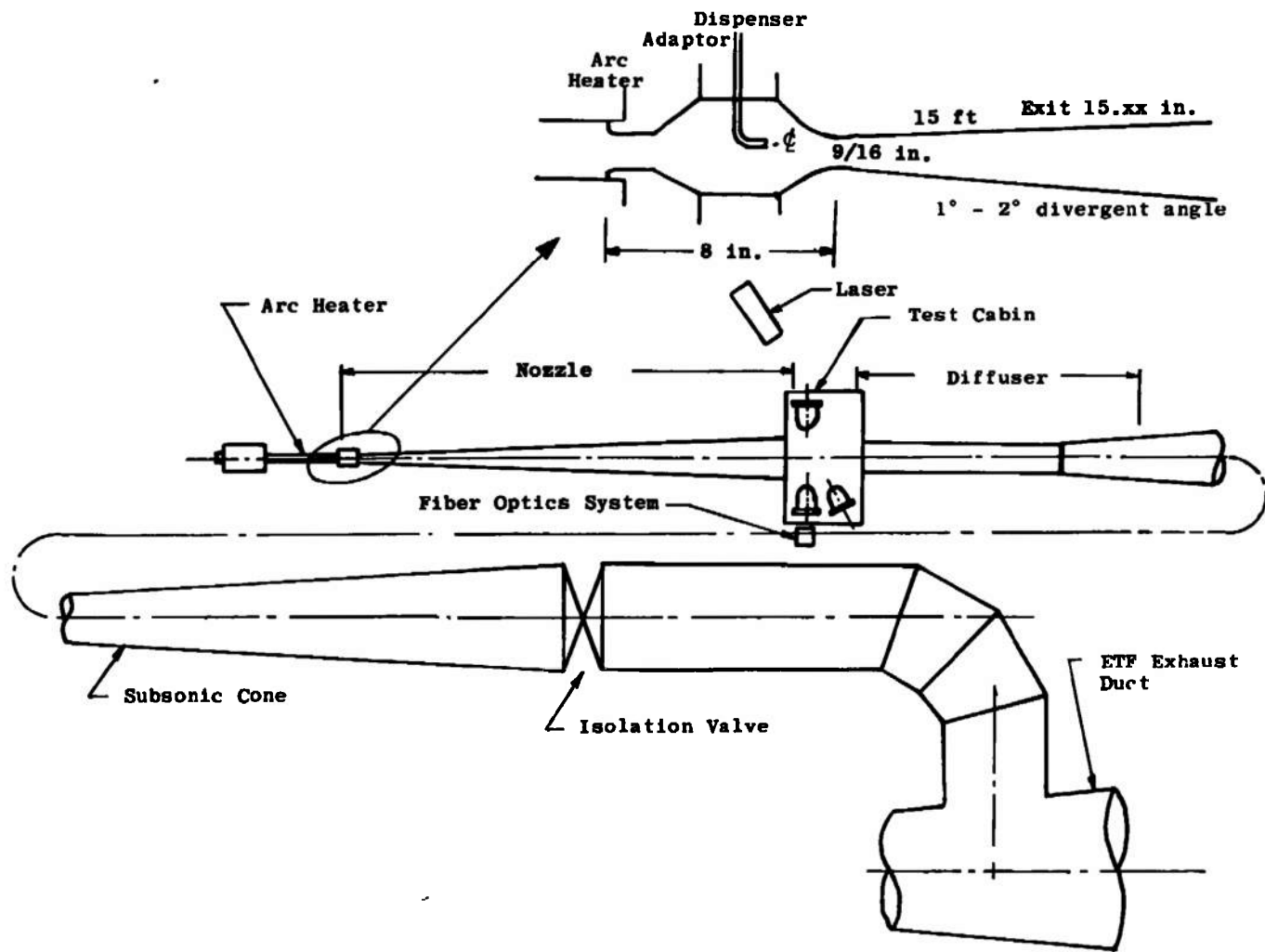
Fig. 31 Layout of Dust Erosion Tunnel
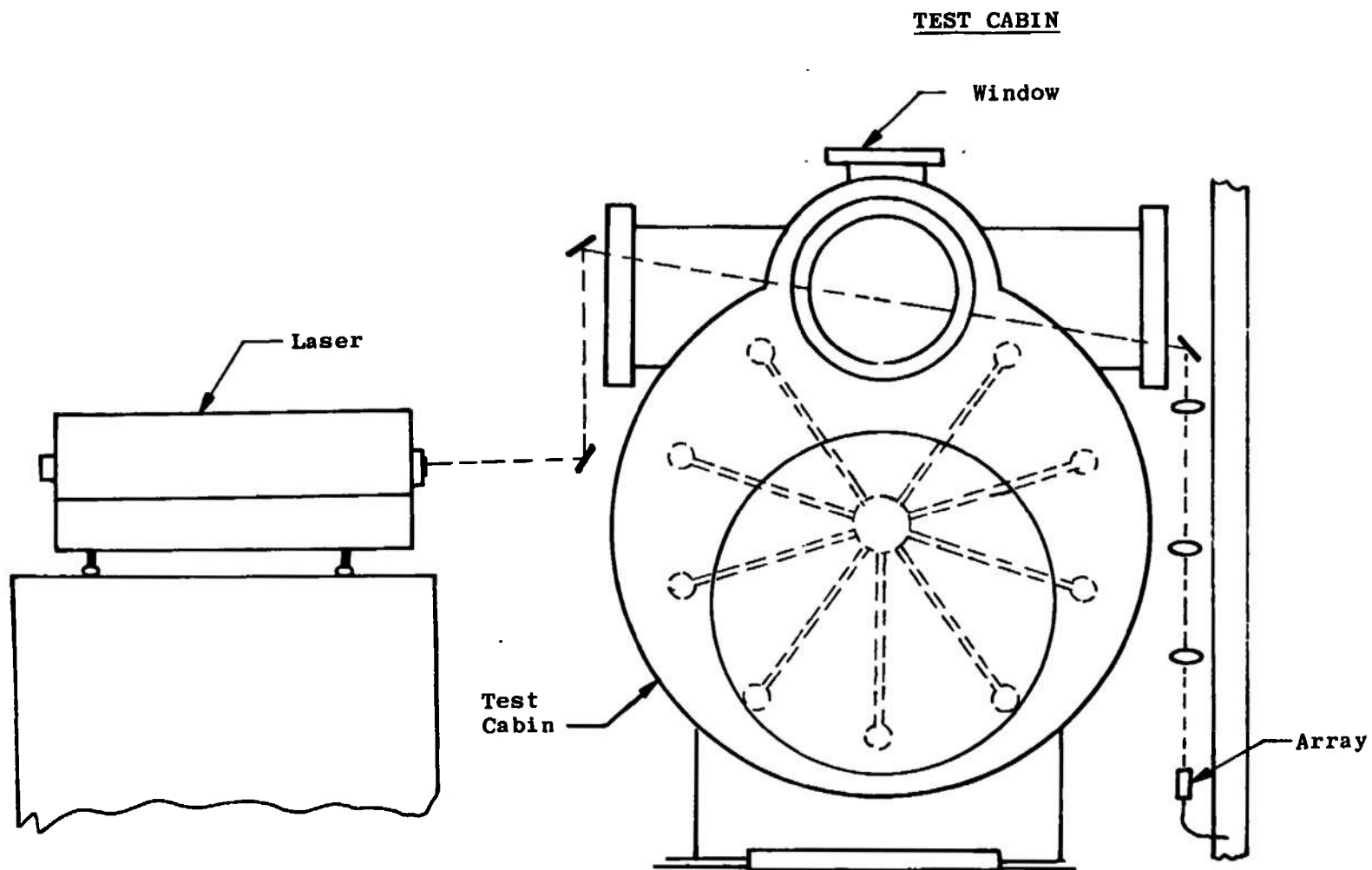
TEST CABIN

Fig. 32 Optical Arrangement through Test Cabin
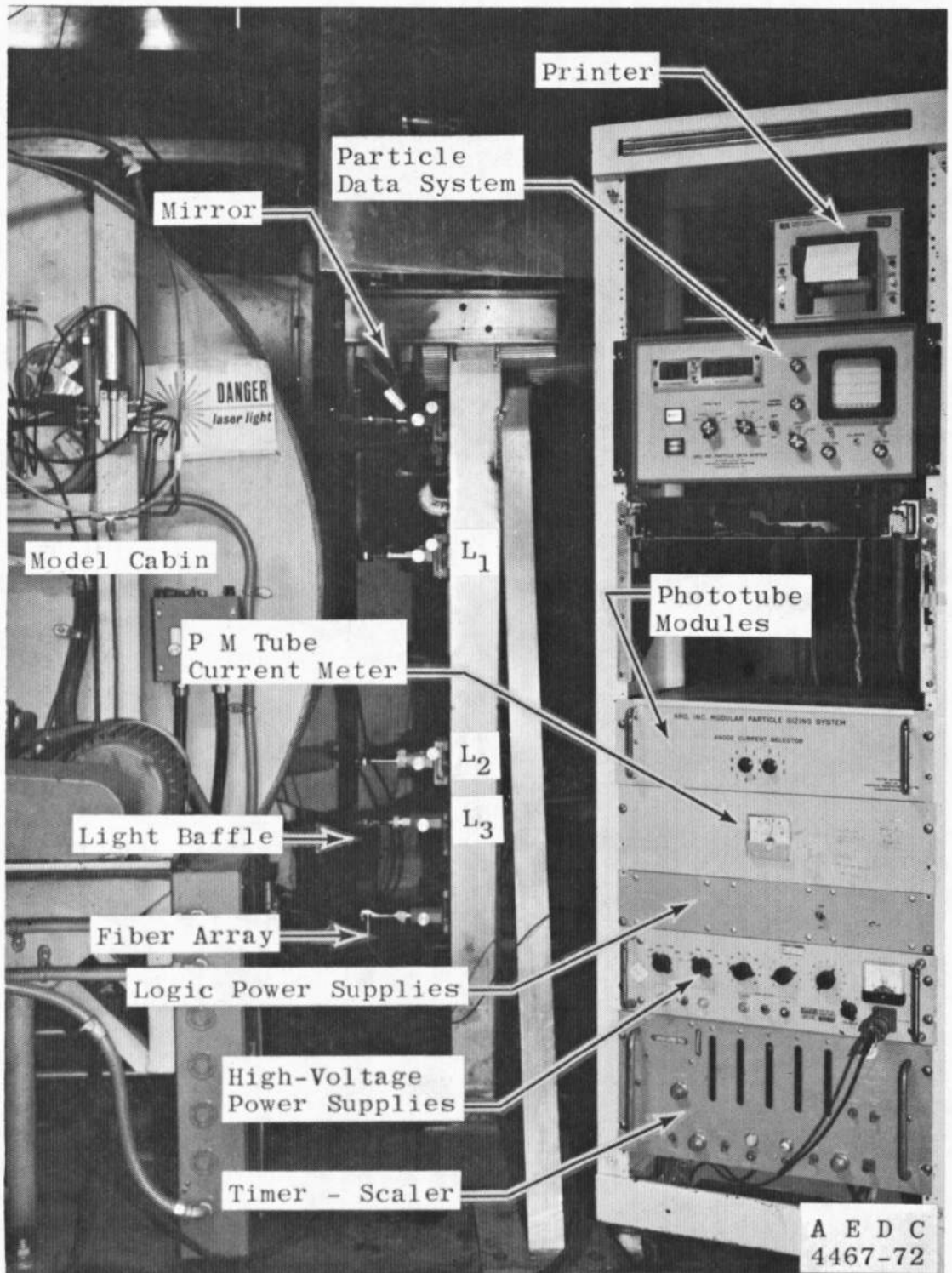
Fig. 33 Fiber Optics Particle Sizer in the Dust Erosion Tunnel
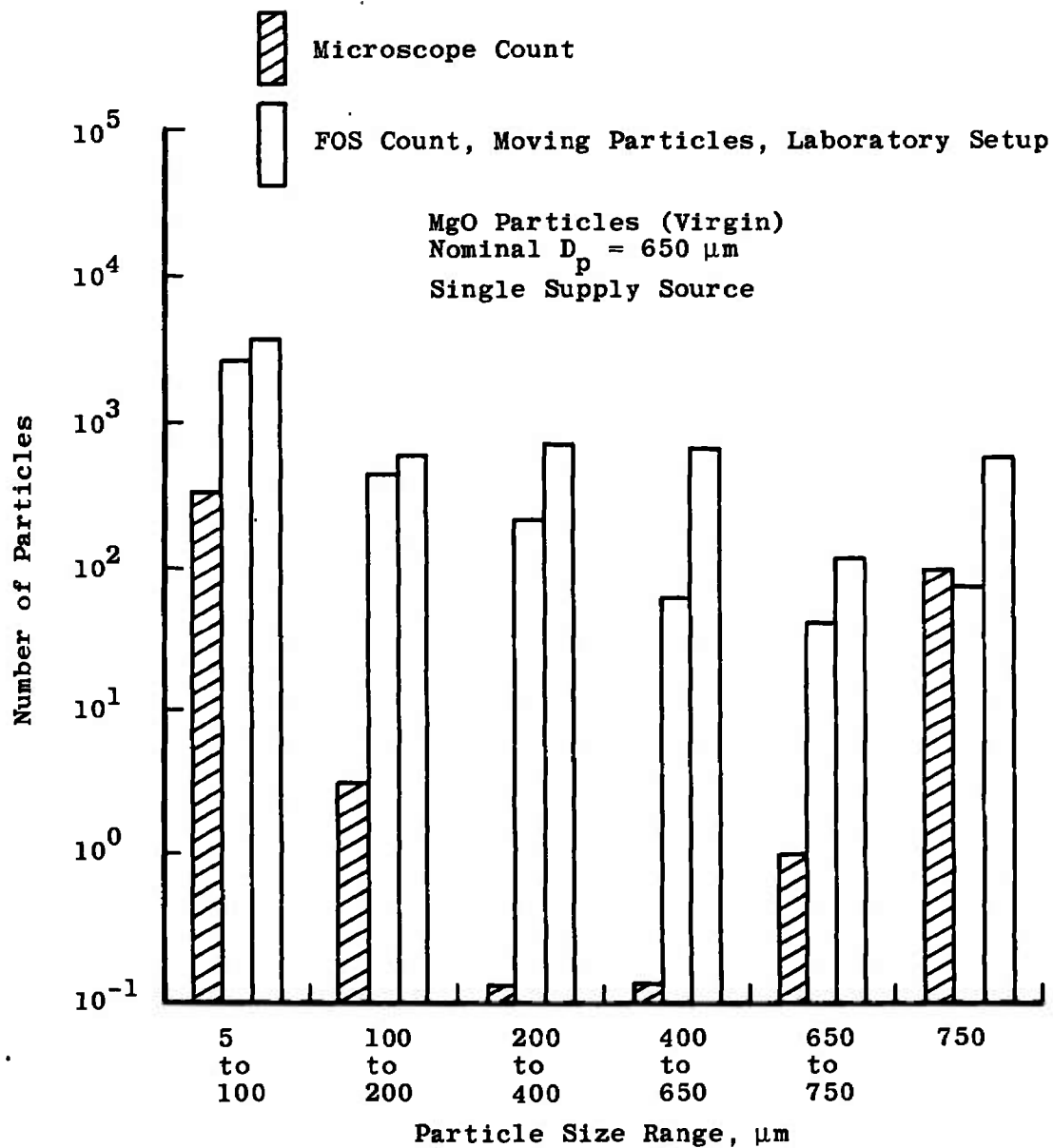
Fig. 34 Comparison of Microscope and FOS Laboratory Particle Counts
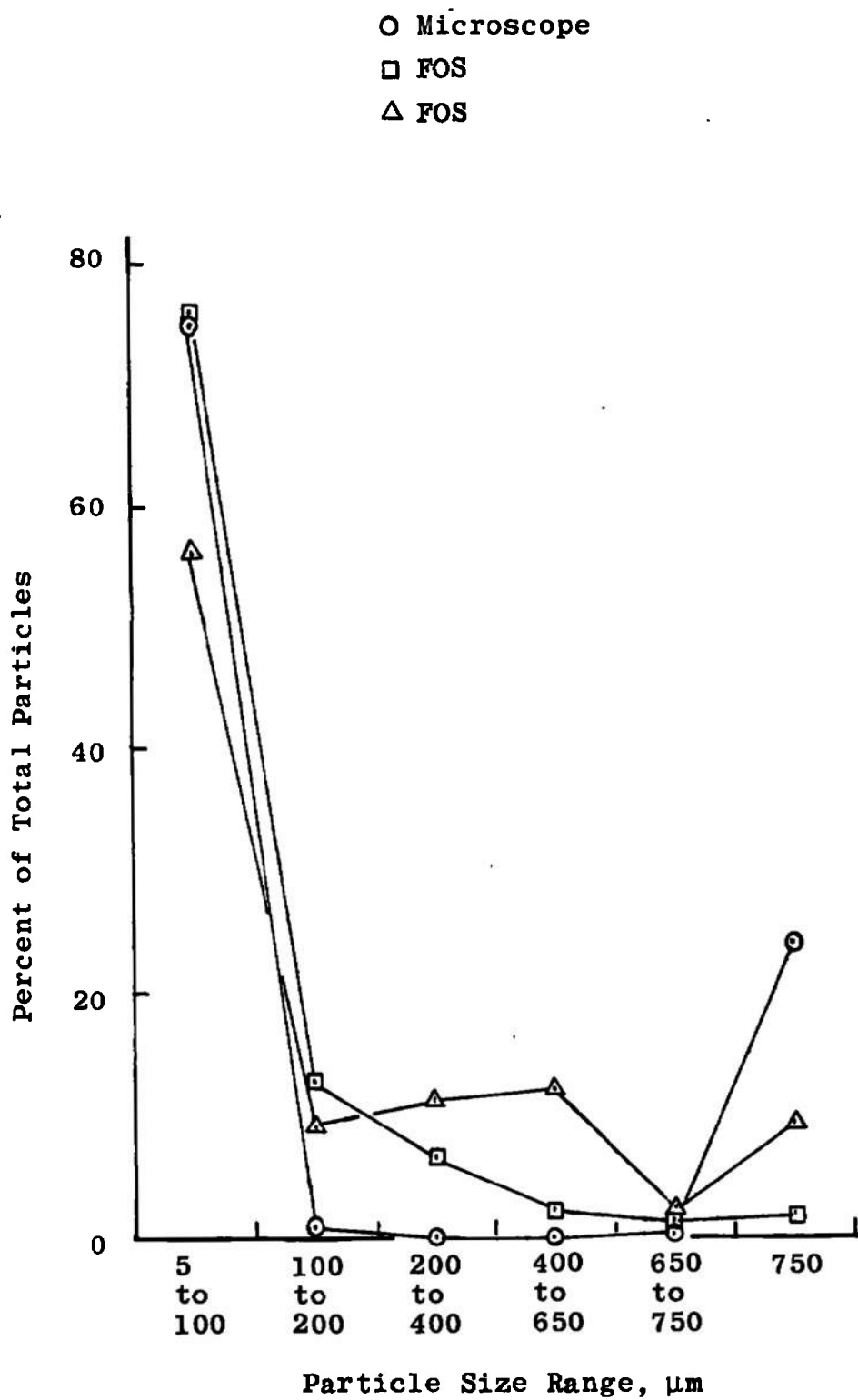
Fig. 35 Percentage Distribution for 650-μm Grit
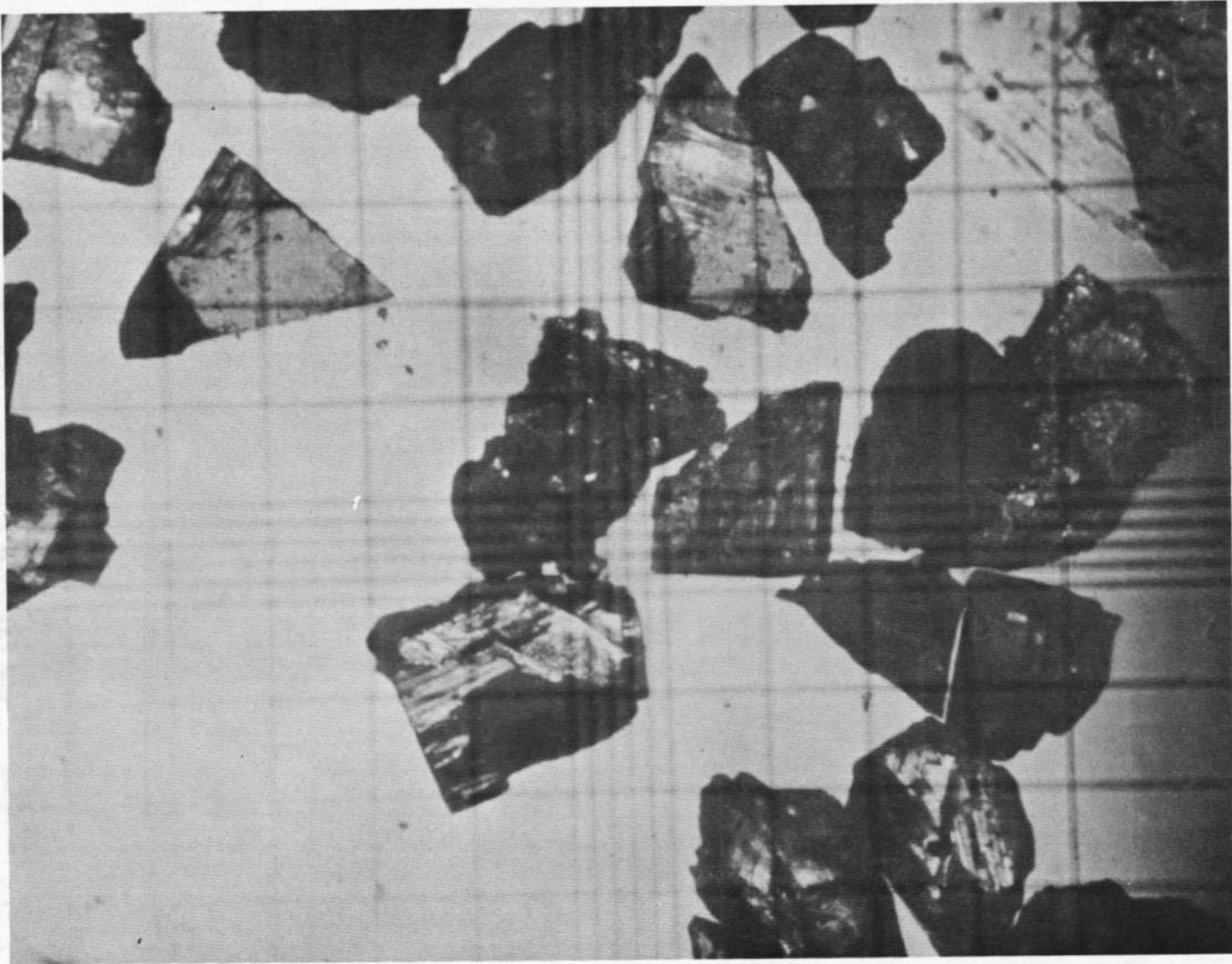
Fig. 36 650-μm Magnesium Oxide
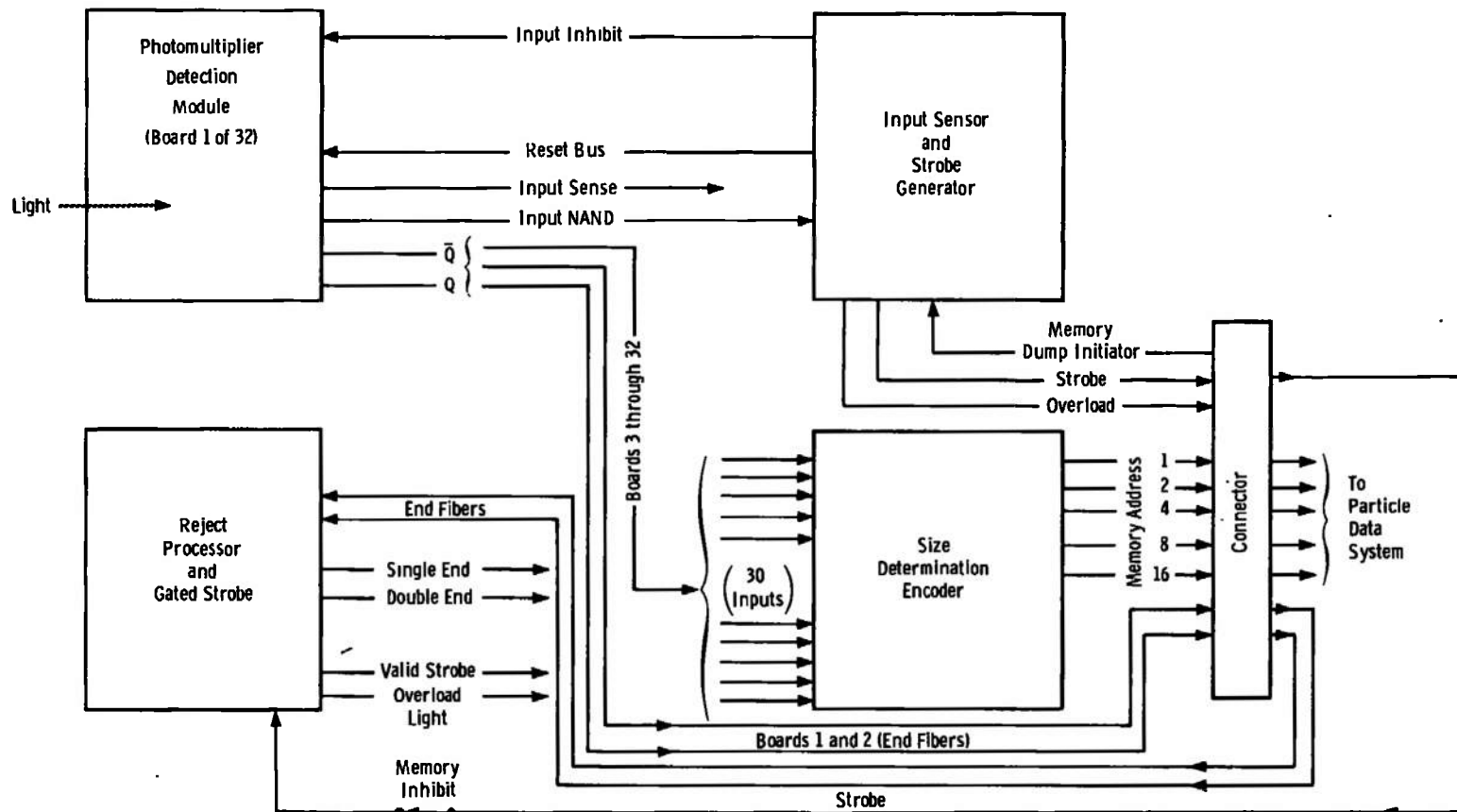
Fig. 37 Fiber Optics System Schematic

Fig. 38 Particle Data System

TABLE I
DATA REDUCTION PROGRAM

FORTRAN IV G LEVEL 20   MAIN   DATE = 73131   11/22/13

```
            C     SET00216  OC  T000  1/13/72  885252  HISTOGRAM PLOT (REVISED)
0001              DIMENSION TITLE(20),D(30),W(30),P(30),OM(31),EL(30),A(30),F(30),
                 1 G(30),OEN(30),R(30),GF(30)
0002              REAL *8 ENO,EN(30),EN31,SEN
0003              DIMENSION BUFF (2178)
0004              CALL CLASS (BUFF,8712)
0005              WRITE(6,2007)
0006        10    READ(5,1000,END=900)TITLE
0007              READ(5,1002)B,T,C,E,V,ELX,THRESH,START
0008              JSTR=START
0009              READ(5,10C2)ENO,EN,EN31
0010              CALL PDF(B,THRESH,D,W,P)
0011              DM(1)=D(1)-.5*B
0012              DO 20 J=2,30
0013        20    OM(J)=.5*(D(J)+D(J-1))
0014              OM(31)=D(30)+.5*B
0015              DO 30 J=1,30
0016              EL(J)=AMIN1(.5*C*O(J)**2/E,ELX)
0017              A(J)=EL(J)*W(J)
0018              F(J)=EN(J)/(P(J)*EL(J)*T)
0019              G(J)=F(J)*(DM(J+1)-DM(J))
0020              OEN(J)=G(J)/V
0021        30    CONTINUE
0022              S=0.
0023              DO 40 J=1,30
0024              IF(J.LT.JSTR)GO TO 39
0025              S=S+G(J)*D(J)**3
0026        39    CONTINUE
0027              R(J)=S
0028        40    GF(J)=G(J)/(B*D(J)**2)
0029              DO 52 J=1,30
0030              R(J)=R(J)/S
0031              IF(GF(J).GT.0.)GO TO 51
0032              GF(J)=-1.E50
0033              GO TO 52
0034        51    GF(J)=ALOG10(GF(J)/S)
0035        52    CONTINUE
0036              SOEN=0.
0037              SG=0.
0038              SEN=0.DO
0039              D10=0.
0040              D20=0.
0041              D30=0.
0042              DO 60 J=JSTR,30
0043              SOEN=SOEN+OEN(J)
0044              SG=SG+G(J)
0045              SEN=SEN+EN(J)
0046              D10=D10+G(J)*O(J)
0047              D20=D20+G(J)*D(J)**2
0048        60    D30=D30+G(J)*O(J)**3
0049              D10=D10/SG
0050              D20=SQRT(O20/SG)
0051              D30=(D30/SG)**.3333333
0052              WRITE(6,2000)TITLE
0053              WRITE(6,2001)
0054              NO=ENO
```

TABLE I (Continued)

```
FORTRAN IV G LEVEL  20                    MAIN                DATE = 73131           11/22/13

  0055              N31=EN31
  0056              WRITE(6,3002)NO,N31,B,T,C,E,V,ELX,THRESH,JSTR
  0057              WRITE(6,2003)
  0058              DO 70 J=1,30
  0059              N=EN(J)
  0060         70   WRITE(6,2002)J,N,D(J),G(J),DEN(J),EL(J),W(J),A(J),R(J),GF(J),F(J)
  0061              N=SEN
  0062              WRITE(6,2005)N,SG,SDEN
  0063              WRITE(6,2006)D10,D20,D30
  0064              WRITE(6,2007)
  0065              CALL GRAB(DM,G,TITLE,'  D ','  J ')
  0066              CALL GRAF(D,F,TITLE,'  D ','  F ')
  0067              GO TO 10
  0068        900   WRITE(6,2004)
  0069              CALL KLASS
  0070              STOP
  0071       1000   FORMAT(20A4)
  0072       1002   FORMAT(6E12.0)
  0073       2000   FORMAT(1H1,19X,20A4)
  0074       2001   FORMAT(1H0,T4,6HSINGLE,T13,6HDOUBLE,T109,8HSTARTING/
                   1                              T4,6HREJECT,T13,6HREJECT,T22,
                   21HB,T34,1HT,T46,1HC,T58,6HLAMBDA,T70,1HV,T82,4HLMAX,T94,6HTHRESH,
                   3T109,7HCHANNEL)
  0075       2002   FORMAT(2I9,1P9E12.4)
  0076       3002   FORMAT(2I9,1P7E12.4,I12)
  0077       2003   FORMAT(1H0,T9,1HI,T17,1HN,T22,1HD,T34,1HJ,T46,7HDENSITY,T58,1HL,
                   1T70,1HW,T82,1HA,T94,1HR,T106,6HLOG(F),T117,9HDIST FUNC)
  0078       2004   FORMAT('0THE END')
  0079       2005   FORMAT(9H0   TOTALS,I9,12X,1P2E12.4)
  0080       2006   FORMAT(1H0,T14,5HD10 =,1PE12.4/T14,5HD20 =,E12.4/T14,5HD30 =,E12.4
                   1)
  0081       2007   FORMAT(1HA)
  0082              END
```

TABLE I (Continued)

```
FORTRAN IV G LEVEL   20                    PDF              DATE = 73131          11/22/13

0001              SUBROUTINE PDF(B,C,D,W,E)
0002              DIMENSION D(30),W(30),E(30),N(30)
0003              T=1.-C
0004              DO 1 J=1,30
0005              D(J)=0.
0006              W(J)=0.
0007        1     N(J)=0
0008              DO 3 L=1,161
0009              X=.1*(L-.5)
0010              DO 2 M=1,321
0011              DH=.05*(M-.5)
0012              AP=DH+X
0013              JP=AP
0014              EP=AP-JP
0015              CALL LUNEY(DH,EP)
0016              IF(EP.GT.T)JP=JP+1
0017              IF(JP.GT.15)GO TO 2
0018              AM=DH-X
0019              JM=AM
0020              IF(AM.LT.0.)JM=JM-1
0021              FM=AM-JM
0022              CALL LUNEY(DH,EM)
0023              IF(EM.GT.T)JM=JM+1
0024              IF(JM.GT.15)GO TO 2
0025              IF(JM.LT.-15)GO TO 2
0026              J=JP+JM
0027              IF(J.LT.1)GO TO 2
0028              N(J)=N(J)+1
0029              D(J)=D(J)+DH
0030        2     CONTINUE
0031        3     CONTINUE
0032              DO 10 J=1,30
0033        10    D(J)=D(J)/N(J)
0034              DO 30 L=1,161
0035              X=.1*(L-.5)
0036              DO 20 K=1,30
0037              DH=D(K)
0038              AP=DH+X
0039              JP=AP
0040              EP=AP-JP
0041              CALL LUNEY(DH,EP)
0042              IF(EP.GT.T)JP=JP+1
0043              IF(JP.GT.15)GO TO 20
0044              AM=DH-X
0045              JM=AM
0046              IF(AM.LT.0.)JM=JM-1
0047              EM=AM-JM
0048              CALL LUNEY(DH,EM)
0049              IF(EM.GT.T)JM=JM+1
0050              IF(JM.GT.15)GO TO 20
0051              IF(JM.LT.-15)GO TO 20
0052              J=JP+JM
0053              IF(J.NE.K)GO TO 20
0054              W(J)=W(J)+1.
0055        20    CONTINUE
0056        30    CONTINUE
```

TABLE I (Continued)

FOFTPAN IV G LEVEL 20   POF   OATE = 73131   11/22/13

```
0057            DO 4 J=1,30
0058            D(J)=2.*B*O(J)
0059            W(J)=.2*B*W(J)
0060       4    F(J)=.02*B*B*N(J)
0061            RETURN
0062            ENO
```

FO*TRAN IV G LEVEL 20   LUNEY   DATE = 73131   11/22/13

```
0001            SUBROUTINE LUNEY(DH,EP)
0002            REAL PI/3.141593/
0003            INTEGER K/0/
0004            D=2.*DH
0005            IF(EP.LT.D)GO TO 10
C006            EP=D*D
0007            RETURN
0008      10    CONTINUE
0009            A=2.*EP
0010            A=A/(A-1.-D)
0011            CT1=1.-A*(EP-D)
0012            CT2=1.-A*(EP-1.)/0
0013            ST1=SQRT(1.-CT1*CT1)
0014            ST2=SQRT(1.-CT2*CT2)
0015            T1=ATAN2(ST1,CT1)
0016            T2=ATAN2(ST2,CT2)
0017            EP=(T1-ST1*CT1+D*D*(T2-ST2*CT2))/PI
0018            RFTURN
0019            ENO
```

TABLE I (Continued)

```
FORTRAN IV G LEVEL   20              GRAB              OATE = 73131        11/22/13

      0001            SUPROUTINE GRAB(A,B,TITLE,LBX,LBY)
      0002            DIMENSION A(31),B(30),TITLE(20),X(120),Y(120),R(2),S(2)
      0003            R(1)=AMIN1(0.,A(1))
      0004            P(2)=A(31)
      0005            S(1)=1.E50
      0006            S(2)=0.
      0007            DO 10 J=1,30
      0008            K=4*(J-1)
      0009            X(K+1)=A(J)
      0010            X(K+2)=A(J)
      0011            X(K+3)=A(J+1)
      0012            X(K+4)=A(J+1)
      0013            Y(K+1)=0.
      0014            Y(K+2)=B(J)
      0015            Y(K+3)=B(J)
      0016            Y(K+4)=0.
      0017            IF(B(J).LE.0.)GO TO 1C
      0018            S(1)=AMIN1(S(1),B(J))
      0019            S(2)=AMAX1(S(2),B(J))
      0020      10    CONTINUE
      0021            CALL CALCMP(1.,1.,0,2)
      0022            CALL  SCALE(2,1,R,1,7,LX,IX,JX,MX,NX)
      0023            CALL  SCALE(2;1,S,0,0,LY,IY,JY,MY,NY)
      0024            MY=1
      0025            NY=1
      0026            JY=IY+6
      0027            CALL AXIS(1.,1.,0.,-13.,LX,IX,JX,MX,NX,4,LBX)
      0028            CALL AXIS(1.,1.,90.,8.0,LY,IY,JY,MY,NY,4,LBY)
      0029            CALL HASH(1.,13.,LX,IX,JX,MX,NX,1.,8.,LY,IY,JY,MY,NY)
      0030            CALL SYMBOL(1.,9.25,.21,TITLE,0.,72)
      0031            CALL LINO(0,0,0,1,X,1.,13.,LX,IX,JX,MX,NX,XN,XX,DX,
     1                          1,Y,1.,  8.,LY,IY,JY,MY,NY,YN,YX,DY)
      0032            YMN=10.**YN
      0033            DO 20 J=1,120
      0034      20    Y(J)=AMAX1(Y(J),YMN)
      0035            CALL LINE(120,0,0,1,X,LX,1,Y,LY)
      0036            RETURN
      0037            ENO
```

71

`

TABLE I (Concluded)

```
FORTRAN IV G LEVEL  20              GRAF              DATE = 73131           11/22/13
    0001            SUBROUTINE GRAF(A,B,TITLE,LBX,LBY)
    0002            DIMENSION A(30),B(30),TITLE(20),X(30),Y(30),R(2),S(2)
    0003            R(1)=AMIN1(0.,A(1))
    0004            R(2)=A(30)
    0005            S(1)=1.E50
    0006            S(2)=0.
    0007            DO 10 J=1,30
    0008            X(J)=A(J)
    0009            Y(J)=B(J)
    0010            IF(B(J).LE.0.)GO TO 10
    0011            S(1)=AMIN1(S(1),B(J))
    0012            S(2)=AMAX1(S(2),B(J))
    0013      10    CONTINUE
    0014            CALL CALCMP(1.,1.,0,2)
    0015            CALL SCALE(2,1,R,1,7,LX,IX,JX,MX,NX)
    0016            CALL SCALE(2,1,S,0,0,LY,IY,JY,MY,NY)
    0017            MY=1
    0018            NY=1
    0019            JY=IY+6
    0020            CALL AXIS(1.,1.,0.,-13.,LX,IX,JX,MX,NX,4,LBX)
    0021            CALL AXIS(1.,1.,90.,8.0,LY,IY,JY,MY,NY,4,LBY)
    0022            CALL HASH(1.,13.,LX,IX,JX,MX,NX,1.,8.,LY,IY,JY,MY,NY)
    0023            CALL SYMBOL(1.,9.25,.21,TITLE,0.,72)
    0024            CALL LINO(0,0,0,1,X,1.,13.,LX,IX,JX,MX,NX,XN,XX,DX,
                   1              1,Y,1.,8.,LY,IY,JY,MY,NY,YN,YX,DY)
    0025            YMN=10.**YN
    0026            DO 20 J=1,30
    0027      20    Y(J)=AMAX1(Y(J),YMN)
    0028            CALL LINE(30,0,0,1,X,LX,1,Y,LY)
    0029            RETURN
    0030            END
```

TABLE II
SAMPLE COMPUTER PRINTOUT

SYMBOLS

B = Bin size (e. g., 3157 μm)
T = Run time in seconds
C = Constant for depth of field
Lambda = Wavelength of source
V = Assumed particle velocity for density calculation
L_{max} = Maximum allowable depth of field
Single reject = Number of times one end fiber was shadowed
Double reject = Number of times both end fibers were shadowed
I = Bin number
D = Particle diameter
N = Number of particles measured in bin
J = Particle flux (number/cm^2-sec-bin)
Density = Particle density (number/cm^3-bin)
L = Length of optical path
W = Effective array width
A = Effective array area
R = Cumulative volume fraction

$$\text{Log }(F) = \frac{\Delta R}{\Delta D \, D^5}$$

Totals are self-explanatory.

D_{10} = Simple average
D_{20} = Area weighted average
D_{30} = Volume weighted average

"Thres," if printed, is the electronic threshold value and has a bearing on the exact D_i used in making calculations.

Log (F) when plotted versus diameter yields a Nukiyama-Tanasawa plot.

The graphs are plots of particle flux. The first is based on predust conditions. A total particle flux of less than 20 particles/cm^2-sec was noted. The particles were about 50 μm in diameter. Note: particles below approximately one bin size are not counted, which may lead to erroneous conclusions. This can be a very important consideration.

TABLE II (Concluded)

#4 X=0,Y=1.1,Z=2.4 9/21/71 ROCKET INJECTOR HOLOGRAPHY COMPARISON

B = 2.5000E-03	T = 7.4445E 00	C = 2.5000E 00	LAMBDA = 6.3280E-05	V = 2.6960E 03
LMAX = 7.4930E-01		SINGLE REJECT = 9610.	DOUBLE REJECT =	612.

I	N	D	J	RHO	L	W	A	R	LOG(F)
1	2549.	2.5000E-03	3.6492E 04	1.3536E 01	1.2346E-01	7.6000E-02	9.3829E-03	2.1939E-04	1.1954E 01
2	2038.	5.0000E-03	7.5422E 03	2.7976E 00	4.9384E-01	7.3500E-02	3.6297E-02	5.8215E-04	1.0667E 01
3	1752.	7.5000E-03	4.4237E 03	1.6406E 00	7.4930F-01	7.1000E-02	5.3200E-02	1.3002E-03	1.0083E 01
4	1768.	1.0000E-02	4.6270E 03	1.7163E 00	7.4930E-01	6.8500E-02	5.1327E-02	3.0806E-03	9.8526E 00
5	1203.	1.2500E-02	3.2676E 03	1.2120E 00	7.4930E-01	6.6000E-02	4.9454E-02	5.5362E-03	9.5077E 00
6	888.	1.5000E-02	2.5070E 03	9.2988E-01	7.4930E-01	6.3500E-02	4.7580E-02	8.7918E-03	9.2342E 00
7	821.	1.7500E-02	2.4128E 03	8.9496E-01	7.4930F-01	6.1000E-02	4.5707E-02	1.3767E-02	9.0837E 00
8	805.	2.0000E-02	2.4669E 03	9.1502E-01	7.4930E-01	5.8500E-02	4.3834E-02	2.1361E-02	8.9774E 00
9	718.	2.2500E-02	2.2985E 03	8.5256E-01	7.4930E-01	5.6000E-02	4.1961E-02	3.1435E-02	8.8443E 00
10	613.	2.5000E-02	2.0541E 03	7.6190E-01	7.4930E-01	5.3500E-02	4.0088E-02	4.3784E-02	8.7040E 00
11	460.	2.7500E-02	1.6170E 03	5.9976E-01	7.4930E-01	5.1000E-02	3.8214E-02	5.6723E-02	8.5173E 00
12	397.	3.0000E-02	1.4674E 03	5.4430E-01	7.4930E-01	4.8500E-02	3.6341E-02	7.1968E-02	8.3996E 00
13	251.	3.2500E-02	9.7819E 02	3.6283E-01	7.4930E-01	4.6000E-02	3.4468E-02	8.4888E-02	8.1539E 00
14	190.	3.5000E-02	7.8302E 02	2.9044E-01	7.4930E-01	4.3500E-02	3.2595E-02	9.7806E-02	7.9929E 00
15	168.	3.7500E-02	7.3457E 02	2.7247E-01	7.4930E-01	4.1000E-02	3.0721E-02	1.1271E-01	7.9052E 00
16	350.	4.0000E-02	1.6297E 03	6.0450E-01	7.4930E-01	3.8500E-02	2.8848E-02	1.5284E-01	8.1953E 00
17	112.	4.2500E-02	5.5773E 02	2.0687E-01	7.4930E-01	3.6000E-02	2.6975E-02	1.6932E-01	7.6769E 00
18	141.	4.5000E-02	7.5454E 02	2.7987E-01	7.4930E-01	3.3500E-02	2.5102E-02	1.9577E-01	7.7585E 00
19	82.	4.7500E-02	4.7420E 02	1.7589E-01	7.4930E-01	3.1000E-02	2.3228E-02	2.1533E-01	7.5098E 00
20	84.	5.0000E-02	5.2838E 02	1.9599E-01	7.4930E-01	2.8500E-02	2.1355E-02	2.4074E-01	7.5123E 00
21	56.	5.2500E-02	3.8612E 02	1.4322E-01	7.4930E-01	2.6000E-02	1.9482E-02	2.6224E-01	7.3337E 00
22	36.	5.5000E-02	2.7463E 02	1.0186E-01	7.4930E-01	2.3500E-02	1.7609E-02	2.7982E-01	7.1453E 00
23	20.	5.7500E-02	1.7073E 02	6.3329E-02	7.4930E-01	2.1000E-02	1.5735E-02	2.9231E-01	6.9003E 00
24	117.	6.0000E-02	1.1338E 03	4.2054E-01	7.4930E-01	1.8500E-02	1.3862E-02	3.3654E-01	7.6855E 00
25	259.	6.2500E-02	2.9019E 03	1.0764E 00	7.4930E-01	1.6000E-02	1.1989E-02	6.5914E-01	8.0582E 00
26	87.	6.5000E-02	1.1553E 03	4.2852E-01	7.4930E-01	1.3500E-02	1.0116E-02	7.8122E-01	7.6241E 00
27	66.	6.7500E-02	1.0756E 03	3.9897E-01	7.4930E-01	1.1000E-02	8.2423E-03	9.0851E-01	7.5603E 00
28	25.	7.0000E-02	5.2727E 02	1.9557E-01	7.4930E-01	8.5000E-03	6.3690E-03	9.7809E-01	7.2191E 00
29	5.	7.2500E-02	1.4939E 02	5.5413E-02	7.4930E-01	6.0000E-03	4.4958E-03	1.0000E 00	6.6409E 00
30	0.	7.5000E-02	0.0	0.0	7.4930E-01	3.5000E-03	2.6225E-03	1.0000E 00	-1.0000E 50

	TOTAL N	D30		TOT RHO					
	16061.	3.1222E-02		3.1673E 01					

TABLE III
INTENSITY DISTRIBUTION PROGRAM

FORTRAN IV G LEVEL   20   MAIN   DATE = 73131   11/23/54

```
          C       SET00244  DC TODD  06/13/72  BB5252  HT BENTLEY
          C       INTENSITY DISTRIBUTION  3RD REVISION  DIRECT METHOD
0001              REAL*8    RA(200),ARE(200),BRE(200),AAG(200),BAG(200),TEN(200)
0002              CALL CLASS('SET00244')
0003              PI=3.141593
00C4              TOL=1.E-4
0005              S=44.
0006              DZ=0.
0007              EM=1.
0308              EL=5.08
0009              F=22.
0010              D=.002
0011              W=4.765E-5
0012              Z=S+DZ
0013              ZP=EM*S
0014              CAYH=PI/W
0015              CAY=2.*CAYH
0016              ELH=.5*EL
0017              A=CAYH*(1./ZP-1./F)
0018              B=A+CAYH/Z
0019              IF(ABS(B*ELH*ELH).LE..01)B=0.
0020              NP=15
0021              NT=20000
0022              WRITE(9,1005)
0023              WRITE(9,1006)S,DZ,EM,EL,F,O,NR
0024              WRITE(9,1007)
0025              WRITE(9,1006)W,Z,ZP,CAY,A,B,NT
0026              NP1=NR-1
0027              NT1=NT-1
0028              DH=.5*D
0029              BC=CAYH*D/Z
0030              RT=1.5*EM*D
0031              DP=RT/NR1
0032              DT=ELH/NT1
0033              TBO=CAY*RT*ELH/ZP
0034              TB1=BC*FLH
0035              TAT=A*ELH*ELH.
0036              TBT=B*ELH*ELH
0037              WRITE(6,1006)TBO,TB1,TAT,TBT
003B              DR=1.D-4
0039              DO 1 J=1,NR
0040              PA(J)=(J-1)*DR
0041              ARE(J)=0.DO
0042              BRE(J)=0.DO
0043              AAG(J)=0.DO
0044        1     BAG(J)=0.DO
0045              PA(15)=30.D-4
0046              C1=CAY/ZP
0047              DC 5  K=1,NT
0048              T=(K-1)*DT
0049              TS=T*T
0050              AR=A*TS
0051              SNA=SIN(AR)
0052              CSA=COS(AR)
0053              AR=B*TS
0054              SNB=SIN(AR)
```

TABLE III (Continued)

```
FORTRAN IV G LEVEL  20                    MAIN           DATE = 73131        11/23/54
  0055            CSB=COS(AR)
  0056            N=1
  C057            X=BC*T
  0058            CALL BESJ(X,N,BJ,TOL,JER)
  0059            IF(JER.EQ.0)GO TO 2
  C060            WPITE(6,9000)X,BJ,TOL,N,JER
  0061      2     BJ1=BJ
  0062            N=0
  0063            C2=C1*T
  0064            DO 4  J=1,NR
  0065            X=C2*RA(J)
  0066            CALL BESJ(X,N,BJ,TOL,JER)
  0067            IF(JER.EQ.0)GO TO 3
  0068            WRITE(6,9000)X,BJ,TOL,N,JER
  0069      3     BJO=BJ
  0070            BBJ=BJO*BJ1
  0071            TBJ=T*BJO
  0072            ARE(J)=ARE(J)+TBJ*CSA
  0073            BRE(J)=BRE(J)+BBJ*SNB
  0074            AAG(J)=AAG(J)+TBJ*SNA
  0075            BAG(J)=BAG(J)+BBJ*CSB
  0076      4     CONTINUE
  0077      5     CONTINUE
  0078            TAN=C1*C1
  0079            C3=DH*DT
  0080            DO 6  J=1,NR
  0081            ARE(J)=DT*ARE(J)
  C082            RPE(J)=C3*BRE(J)
  0083            AAG(J)=DT*AAG(J)
  0084            BAG(J)=C3*BAG(J)
  0085            TEN(J)=TAN*((ARE(J)-BRE(J))**2+(AAG(J)+BAG(J))**2)
  0086      6     CONTINUE
  0087            CALL SCALEX(NR,RA,' R2 ')                                    PLOT
  0088            CALL GRAF(RA,ARE,'REAL A',6)
  0089            CALL GRAF(RA,BRE,'REAL B',6)
  0090            CALL GRAF(RA,AAG,'IMAGINARY A',11)
  0091            CALL GRAF(RA,BAG,'IMAGINARY B',11)
  0092            CALL GRAF(RA,TEN,'INTENSITY',9)                             PLOT
  0093            WRITE(6,1004)
  0094            CALL CLASS('SET00244')
  0095            STOP
  C096     1004   FORMAT(' THE END')
  0097     1005   FORMAT(4X,1HS,11X,2HOZ,10X,1HM,11X,1HL,11X,1HF,11X,1HD,13X,2HNR)
  0098     1006   FORMAT(1P6E12.4,18)
  0099     1007   FORMAT(4X,6HLAMBDA,6X,1HZ,11X,2HZP,10X,1HK,11X,1HA,11X,1HB,13X,2HN
                 1T)
  0100     9000   FORMAT(1P3E14.6,2I14)
  0101            END
```

TABLE III (Continued)

```
FORTRAN IV G LEVEL   20              GRAF              OATE = 73131          11/23/54
    0001            SUBROUTINE GRAF(X,Y,LABY,NL)
    0002            DIMENSION X(1),Y(1),LABY(1),LAB(20)
    0003            INTEGER K/2/
    0004            CALL SCALE (N,K,Y,5,4,LY,IY,JY,MY,NY)
    0005            CALL CALCMP (1.,1.,0,2)
    0006            REWIND 9
    0007            READ(9,210)LAB
    0008            CALL SYMBOL(1.,10.25,.19,LAB,0.,80)
    0009            READ(9,210)LAB
    0010            CALL SYMBOL(1.,10.00,.19,LAB,0.,80)
    0011            READ(9,210)LAB
    0012            CALL SYMBOL(1.,9.50,.19,LAB,0.,80)
    0013            READ(9,210)LAB
    0014            CALL SYMBOL(1.,9.25,.19,LAB,0.,80)
    0015            CALL HASH(1.,13.,LX,IX,JX,MX,NX,1.,8.,LY,IY,JY,MY,NY)
    0016            CALL AXIS(1.,1.,0.,-13.,LX,IX,JX,MX,NX,4,LABX)
    0017            CALL AXIS(1.,1.,90.,8.,LY,IY,JY,MY,NY,NL,LABY)
    0018            CALL LINO(N,0,0,K,X,1.,13.,LX,IX,JX,MX,NX,01,02,03,
                   1           K,Y,1.,8.,LY,IY,JY,MY,NY,D4,DY,D6)
    0019            RETURN
            C
    0020            ENTRY SCALEX(N1,X,LBX)
    0021            N=N1
    0022            LABX=LBX
    0023            CALL SCALE(N,K,X,5,7,LX,IX,JX,MX,NX)
    0024            RETURN
    0025       210  FORMAT(20A4)
    0026            END
```

```
FORTRAN IV G LEVEL   20              BESJ              DATE = 73131          11/23/54
    0001            SUBROUTINE BESJ(X,N,BJ,0,IER)                    BESJ 042
    0002            REAL PI/3.141593/
    0003            BJ=.0                                            BESJ 044
    0004            IEP=0
    0005            IF(N)10,20,20                                    BESJ 045
    0006       10   IER=1                                           BESJ 046
    0007            RETURN                                           BESJ 047
    0008       20   IF(X)30,25,31
    0009       25   IF(N.EQ.0)BJ=1.
    0010            RETURN
    0011       30   IER=2
    0012            RETURN                                           BESJ 050
    0013       31   IF(X.GT.25.)GO TO 310
    0014            IF(X-15.)32,32,34
    0015       32   NTEST=20.+10.*X-X** 2/3                          BESJ 052
    0016            GO TO 36                                         BESJ 053
    0017       34   NTEST=90.+X/2.                                  BESJ 054
    0018       36   IF(N-NTEST)40,38,38                             BESJ 055
    0019       38   IER=4                                           BESJ 056
    0020            RETURN                                           BESJ 057
```

TABLE III (Concluded)

```
FORTRAN IV G LEVEL  20              BESJ          DATE = 73131        11/23/54

0021        40 IFR=0                                                  BESJ 058
0022           N1=N+1                                                 BESJ 059
0023           RPREV=.0                                               BESJ 060
0024           IF(X-5.)50,60,60                                       BESJ 064
0025        50 MA=X+6.                                                BESJ 065
0026           GO TO 70                                               BESJ 066
0027        60 MA=1.4*X+60./X                                         BESJ 067
0028        70 MB=N+IFIX(X)/4+2                                       BESJ 068
0029           MZERO=MAXO(MA,MB)                                      BESJ 069
0030           MMAX=NTEST                                             BESJ 073
0031       100 DO 190 M=MZERO,MMAX,3                                  BESJ 074
0032           FM1=1.0E-28                                            BESJ 078
0033           FM=.0                                                  BESJ 079
0034           ALPHA=.0                                               BESJ 080
0035           IF(M-(M/2)*2)120,110,120                               BESJ 081
0036       110 JT=-1                                                  BESJ 082
0037           GO TO 130                                              BESJ 083
0038       120 JT=1                                                   BESJ 084
0039       130 M2=M-2                                                 BESJ 085
0040           DO 160 K=1,M2                                          BESJ 086
0041           MK=M-K                                                 BESJ 087
0042           BMK=2.*FLOAT(MK)*FM1/X-FM                              BESJ 088
0043           FM=FM1                                                 BESJ 089
0044           FM1=BMK                                                BESJ 090
0045           IF(MK-N-1)150,140,150                                  BESJ 091
0046       140 BJ=BMK                                                 BESJ 092
0047       150 JT=-JT                                                 BESJ 093
0048           S=1+JT                                                 BESJ 094
0049       160 ALPHA=ALPHA+BMK*S                                      BESJ 095
0050           BMK=2.*FM1/X-FM                                        BESJ 096
0051           IF(N)180,170,180                                       BESJ 097
0052       170 BJ=BMK                                                 BESJ 098
0053       180 ALPHA=ALPHA+BMK                                        BESJ 099
0054           BJ=BJ/ALPHA                                            BESJ 100
0055           IF(ABS(BJ-BPREV)-ABS(D*BJ))200,200,190                 BESJ 101
0056       190 BPREV=BJ                                               BESJ 102
0057           IFR=3                                                  BESJ 103
0058       200 RETURN                                                 BESJ 104
0059       310 BJ=SQRT(2./(PI*X))*COS(X-.5*PI*(N-.5))
0060           RETURN
0061           END                                                   BESJ 105
```

DOCUMENT CONTROL DATA - R & D

(Security classification of title, body of abstract and indexing annotation must be entered when the overall report is classified)

1 ORIGINATING ACTIVITY (Corporate author)	2a. REPORT SECURITY CLASSIFICATION
Arnold Engineering Development Center Arnold Air Force Station, Tennessee 37389	UNCLASSIFIED
	2b GROUP N/A

3 REPORT TITLE

FIBER OPTICS PARTICLE-SIZING SYSTEM

4 DESCRIPTIVE NOTES *(Type of report and inclusive dates)*

Final Report - July 1971 to June 1972

5 AUTHOR(S) *(First name, middle initial, last name)*

H. T. Bentley, ARO, Inc.

6 REPORT DATE	7a. TOTAL NO OF PAGES	7b. NO OF REFS
September 1973	86	7

8a CONTRACT OR GRANT NO	9a. ORIGINATOR'S REPORT NUMBER(S)
b PROJECT NO	AEDC-TR-73-111
c Program Element 65802F	9b OTHER REPORT NO(S) *(Any other numbers that may be assigned this report)*
d	ARO-OMD-TR-73-48

10 DISTRIBUTION STATEMENT

Approved for public release; distribution unlimited.

11 SUPPLEMENTARY NOTES	12 SPONSORING MILITARY ACTIVITY
Available in DDC	Arnold Engineering Development Center Air Force Systems Command Arnold Air Force Station, Tenn 37389

13 ABSTRACT

   A fiber optics particle-sizing system is discussed with respect to theory of operation and data acquisition and reduction techniques. The system utilizes a shadow-graphic technique to determine the dimensions and numbers of particles moving in a flow field. The system is digital in nature. Particles pass through a collimated laser beam and are imaged onto a linear array by a coaxial lens. The array is composed of the exposed ends of a fiber optics bundle which serves as a "link" between the array plane and the sensing photo-detector modules. Being an imaging device, it can measure a wide range of particle sizes through the proper selection of optics. Sizes ranging from 2 to 1500 μ m have been measured in the course of this project. Comparisons of holographic data of a liquid rocket injector and of water spray nozzles are made with the fiber optics system.

DD FORM 1473
(1 NOV 65)

14 KEY WORDS	LINK A		LINK B		LINK C	
	ROLE	WT	ROLE	WT	ROLE	WT
particle size distribution						
shadowgraph						
flow distribution						
lasers						
fiber optics						
storage heaters						
contamination						